NTNU – Trondheim
Norwegian University of
Science and Technology

A high resolution flood forecasting tool and hydropower simulator

Niccolò Bonfadini

Hydropower Development
Submission date: December 2014
Supervisor: Oddbjørn Bruland, IVM

Norwegian University of Science and Technology
Department of Hydraulic and Environmental Engineering

FOREWORD

This report, which is entitled *"A high resolution flood forecasting tool and hydropower simulator"*, is submitted to the Department of Hydraulic and Environmental Engineering at the Norwegian University of Science and Technology as a partial fulfilment of the requirements of the Master of Science in Hydropower Development.

This thesis was carried out from July 2014 to December 2014 at Norwegian University of Science and Technology under the supervision of Prof. Oddbjørn Bruland. The author hereby declares that the work presented in this report is his own and significant outside input is acknowledged appropriately.

Niccolo Bonfadini
December 2014
Trondheim, Norway

Acknowledgments

This thesis has been possible thanks to the support and interest of Oddbjørn Bruland that have introduced me to the topics presented here and that gave me the possibility to grow professionally and academically, to the people in Statkraft (Gaute Lappegard, Robert Von Hirsch, John Burkhart, Helset Sigbjørn, Knut Sand) for their help and support throughout the months of my internship, to Sjur Kolberg at SINTEF thanks to whom I have learned the tools used in this work, to Knut Alfredsen for his insights and support when needed to further improve the topics of the thesis and to Thomas Nipen at DNMI for his help on questions regarding the meteorological models.

I am grateful to my family for allowing me to follow my dream of coming to Norway and pursue this Master and to my friend Matteo Bolzoni and all the other people met here that have made my stay in Trondheim so perfect.

Lastly I would like to express my deepest gratitude to Agota Lorincz for having made the last months the best of my life.

Abstract

Hydrological forecasting is a fundamental science both for hydropower producers, that are interested to know the availability of water in the coming hours and days for production planning purposes, and for municipalities that need to be prepared for flood situations. In the last years the introduction and spreading of distributed hydrological modelling have increased the development and research possibilities. At the same time, meteorological models are becoming more advanced and with increased simulation resolution. This study aims at incorporating three forecast outputs (temperature, wind and precipitation) of the 2.5x2.5Km resolution AROME meteorological model with a six hours updating cycle into a hydrological distributed model. The aim is to evaluate the reliability of such six hours forecasts within the hydrological field by calibrating a model with 20 months of archived data. The results have shown similar performances as compared to using observed data from meteorological stations. Furthermore, a simple hydropower simulating system (HySS) has been introduced to include the artificial components of a hydropower scheme to compute the effective runoff in every point in space. Two case studies were then analysed to assess the reliability of the HySS routine and that of the spatial variability of the forecasted precipitation; the tests have showed very good results of the HySS routine, being able to closely simulate storage and water levels at a system of reservoir in the upper Nea-Nidelva catchment, while, on the other side, highlighting the limitations in the spatial accuracy of the precipitation variable which proved to be unsufficient for hydrological forecasts in localized areas.

Table of Contents

Foreword I

Acknowledgments II

Abstract III

List of Figures VII

List of Tables IX

List of Abbreviations X

Chapter 1 Introduction 1

1.1 Background 1

1.2 Objective of the study 2

1.3 Scope of the study 2

1.4 Methodologies and tools 2

1.5 Structure of the thesis 3

Chapter 2 Data Analysis and Processing 4

2.1 Study Area 4

2.2 Distributed Geographical Inputs 5

2.2.1 Catchments 5

2.2.2 Digital Elevation Map (DEM) 5

2.2.3 Forests Raster 5

2.2.4 Glaciers Raster 6

2.2.5 Landuse 6

2.3 Network Inputs 6

2.3.1 Radiation Data 7

2.3.2 Wind Data 7

2.3.3 Precipitation and Temperature Data 8

2.3.4 Relative Humidity Data 10

2.3.5 River Discharge 10

2.4 Distributed Meteorological Inputs 12

2.4.1 Data Processing 13

2.4.2 Precipitation 13
2.4.3 Temperature 15
2.4.4 Wind 17
Chapter 3 Models Setups and Performances 19
3.1 ENKI 19
3.2 Model Structure 19
3.2.1 Interpolation Routines 20
3.2.2 Priestley-Taylor Evapotranspiration Equation 20
3.2.3 Energy Balance Snow Routine 21
3.2.4 Response Routine 21
3.3 Parameter Calibration 22
3.3.1 Calibration Parameters 22
3.3.2 Objective Function 22
3.3.3 Calibration Algorithm 23
3.4 The Kirchner's Routine 23
3.4.1 A Priori Estimation of the Kirchner's Parameters 25
3.5 PIHM Calibration Performance 26
3.5.1 Parameters Sensitivity 29
3.6 DIHM Calibration Performance 30
3.6.1 Parameters' Sensitivity 31
3.7 Apriori Estimation of Parameters vs Calibration 32
3.8 Why a Minimalistic Approach 33
Chapter 4 Flood Forecasting System 35
4.1 Point flow forecasting 35
4.1.1 Background conditions 35
4.1.2 Purposes 35
4.1.3 Needed development 36
4.2 The hydropower system simulator (HySS) 36
4.2.1 Main components 37
4.2.2 Theory of the HySS routine 37
4.3 Future Developments 39

Chapter 5 Study Cases 40
5.1 Trondheim's Flood 40
5.1.1 Event Description 40
5.1.2 Simulating with AROME data 42
5.2 The upper Nea-Nidelva hydropower system 44
Chapter 6 Conclusion and Recommendations 48
6.1 Conclusion 48
6.2 Recommendations 49
References 50

List of Figures

Figure 1. Overview of the study area. The letters after the station names refer to the data collected (Q = discharge, P = precipitation, T = temperature, H = humidity). 4

Figure 2. An example of a raster map, the forest cover. Green areas represent forested areas 5

Figure 3. Example of IDW interpolation for precipitation observation for the 2nd March 2013. 8

Figure 4. A plot of the cumulative precipitation for all the stations. Generally, with the exception of Svarttjørnbekken, the observations follow the same patterns..... 9

Figure 5. Cumulative temperature (left) and variations in annual mean temperatures with elevation. 9

Figure 6. Output from the Bayes Kriging interpolation routine for the temperature for the 2nd March 2013. 10

Figure 7. Observed river discharge for Gaula and Svarttjørnbekken 11

Figure 8. Resultant local Gaulfoss discharge and its negative values. 12

Figure 9. (left) Time series representing the average precipitation of the Gaulfoss catchment over the simulation period and (right) cumulative precipitation with attempted correction.14

Figure 10. An example of AROME's precipitation raster, as simulated for the 2nd March 2013. Cloud systems are represented and precipitation acquires a more local connotation. . 15

Figure 11. Temperature time series (left) of average daily temperatures and cumulative daily temperatures (right) for Gaulfoss (top) and Svarttjørnbekken (bottom) 16

Figure 12. AROME temperature input for the 2nd March 2013. If compared to the interpolation from the Bayesian Kriging interpolation routine (see Chapter) the results show a high level of similarity. 17

Figure 13. (left) Coefficient (C_f) to transform a 10m height wind measure (u_z) into the standard 2m and its equation. (right) Average hourly windspeed for Gaulfoss and Svarttjørnbekken catchments. 18

Figure 14. Schematic representation of PIHM and DIHM model stacks. 20

Figure 15. Schematic representation of the Kirchner Routine inputs, outputs and states.... 23

Figure 16. Flow recession plot in a logarithmic view and its linear interpolation..... 25

Figure 17. Simulated and Observed Runoffs for the PIHM model with all stations included. 27

Figure 18. Flow simulation without Statkraft's and NVE's stations. 28

Figure 19. Parameter sensitivity analysis for Gaulfoss: only lnTau3 has a clear value that achieves the best model performance. For the other three variables, only a more general optimal area can be identified..... 29

Figure 20. Flow simulation with distributed model including precipitation, temperature and wind measurements..... 31

Figure 21. Parameter sensitivity for the Gaulfoss catchment in the setup including wind speeds..... 32

Figure 22. The figure visually shows how the number of runs necessary to cover every possible combination of the parameter space increases with the number of calibration variables and discretization level. 34

Figure 23. Visual representation of the possible applications of a comple point inflow model. 36

Figure 24. (left) Border cells contain the integer ID value that the center cell would be assigned with if water would flow towards their direction. (right) Conceptual representation of a cell of the "Flow Direction" raster..... 37

Figure 25. Conceptual representation of the HySS routine components..... 38

Figure 26. Overview of the study case area. 40

Figure 27. Precipitation and corresponding runoff responses for two timesteps, with and without distributed data. 43

Figure 28. Schematical representation of the simulated hydropower system. 44

Figure 29. Normalized level-spill and level-storage curves. 46

Figure 30. Storage (left, Sylsjøen) and water levels (right, Nesjøen) for a 10days snowmelt period. 46

List of Tables

Table 1. Stations used in the model, along with their UTM32N coordinates and elevations. 6

Table 2. R2 performances of the PIHM model with all available stations..... 26

Table 3. Nash-Sutcliffe coefficients for the five catchment using only DNMI's stations..... 28

Table 4. Comparison of simulation performances between two different distributed model setups and the model with observation inputs (T=temperature, P=precipitation,W=wind) 30

Table 5. Nash-Sutcliffe coefficients for the PIHM model with estimated Kirchner parameters. 33

Table 6. Return periods for different rain intensity and time frames. Source: Trondheim Kommune. 41

Table 7. Observed precipitation by DNMI's stations in Trondheim. Voll shows daily record. 42

List of Abbreviations

AROME	Application of Research to Operations at Mesoscale
°C	Degrees centigrade
DEM	Digital Elevation Model
DIHM	Distributed Inputs Hydrological Model
DNMI	Den Norske Meteorologisk Institutt
GDAL	Geospatial Data Abstraction Library
GIS	Geographical Information Software
HBV	Hydrologiska Byråns Vattenbalansavdelning
HySS	Hydropower Simulator System
IDW	Inverse Distance Weight
KPa	Kilo Pascal
lnR2	Natural logarithm of Nash-Sutcliffe coefficient
m/s	Meters per second
m3/s	Cubic meters per second
mill.m3	Millions cubic meters
MJ	Mega Joule
NetCDF	Network Common Data From
PIHM	Point Inputs Hydrological Models
rad	Radiants
R^2	Nash-Sutcliffe coefficient

Chapter 1

Introduction

1.1 Background

Hydrological models aim at representing the hydrological processes and cycles through stochastic or process based methodologies. In Norway the dependence on hydropower resources for energy production and its deregulated market have pushed the major hydropower companies to implement and automatize hydrological models in order to provide as accurate as possible forecasts for production planning. In the last decades, lumped models as the HBV (Bergstrøm & Forsman, 1973) were the most widely spread and used models due to the simplicity of the underlying concepts and applicability. These models represent a catchment as a single entity with fixed averaged characteristics such as elevation, forest and lake covers. Modern developments have seen the creation of distributed model frameworks such as ENKI (Bruland, Lena S., Engeland, & Kolberg, 2009), where a catchment is divided in cells of fixed resolution (usually 1x1km) each one holding those informations that were before attributed to the whole area. ENKI enables to use the full potential of added data from a variety of sources, such as GIS data and satellite imagery, for example for snow coverage studies (Kolberg, 2006) and land use classification (Friedl & al., 2002). One of the main uses of hydrological models is in forecasting, using as inputs the outputs from meteorological models. Previous studies conducted on the topic have highlighted the limitation and uncertainties introduced by the forecasted precipitation variables (Bartholmes & Todini, 2005) from the HIRLAM meteorological model (Källén, 1996). Such conclusions have created the need to verify the possibilities of improving the quality of the hydrological forecasts by using the higher resolution AROME model (Seity, et al., 2011). More accurate forecasting models are important for predicting floods; though in a Norwegian setting where most of the catchments are regulated by the presence of reservoir and water diversions, it is important to include in the model these components in order to have a realistic representation of the system.

1.2 Objective of the study

The main purpose of this master's thesis is to create high resolution distributed flow forecasts in order to provide a tool capable of predicting the amount of water that will flow in a specific point in space with a 1x1km resolution. It will be achieved by using as inputs the most advanced meteorological models available at present covering the Norwegian territory. The reason why advanced distributed meteorological inputs are analysed in this dissertation is to provide the most accurate as possible estimate of runoff. Also, the high definition will allow to model the regions at a scale that is smaller than that of the catchment, making it possible to catch and model the response of areas that lay between two measuring stations, that would not be considered with a normal lumped model based on point inputs.

Thus, the tool will produce forecasts of any potential hazard or damages that floods may cause to humans and structures; by defining, for example, the maximum flow capacity of a culvert, it will make it possible to analyse if the integrity of a structure is at risk.

1.3 Scope of the study

To achieve such objective, the work will have the following points as scope:

- Retrieving of meteorological, geographical and hydrological inputs to feed the model.
- Data processing: programming of a script that enables to extract the huge amount of data that comes from the distributed meteorological inputs.
- Setup and calibration of a distributed model that allows comparisons of the performance achieved by using distributed meteorological inputs as opposed to point-networks.
- Evaluation of the forecast simulations.
- Programming of a tool that enables to forecast the inflow for every needed point in space
- Evaluation of the flood forecasting results and comparison to historical events.

1.4 Methodologies and tools

Most of the research on the topic will be carried out using the ENKI distributed hydrological modelling framework. It is not strictly a hydrological modelling software as it provides a general foundation for developing and running one's routines and tests. ENKI allows to program new models through C++ language, and being open source allows for a free spreading and increase of information and tools among the hydrological community. Thanks to its flexible characteristics it has proven itself valuable in a number of Master's and PhD's thesis. In particular, during my work I have utilized its advantageous feature to

create routines capable of reading distributed inputs and create flood forecasts at specific points in space.

The ENKI tool has been coupled with Geographical Information Softwares such as ArcGIS; its use has been necessary in order to provide ENKI with the required raster files describing catchment properties, such as elevation, mapping of lakes, forests and glaciers. For a more in depth analysis of the model structure and characteristics and the raster files produces in ArcGIS, refer to Chapter 2.4.

1.5 Structure of the thesis

The focus, and thus the structure of the thesis, will be around the following two main steps:

- Assessing the advantages of using the outputs from high resolution meteorological models as inputs to the hydrological tool
- Evaluating the reliability of the flood warning system by comparing simulated results with historical events.

Chapter 2

Data Analysis and Processing

2.1 Study Area

The study area lays in the region of Sør-Trøndelag, in Norway; here, two main catchments have been selected for the analyses: Svarttjørnbekken and Gaula. These two regions were found to be ideal for testing purposes due to their unregulated characteristics and the fact that they are very different in size and density of the station network. Svarttjørnbekken has an area of approximately 3.4 Km^2, as opposed to the 3500 Km^2 of the Gaula catchment. Furthermore Svarttjørnbekken counts a total of 1 temperature and precipitation stations versus the 10 of Gaula.

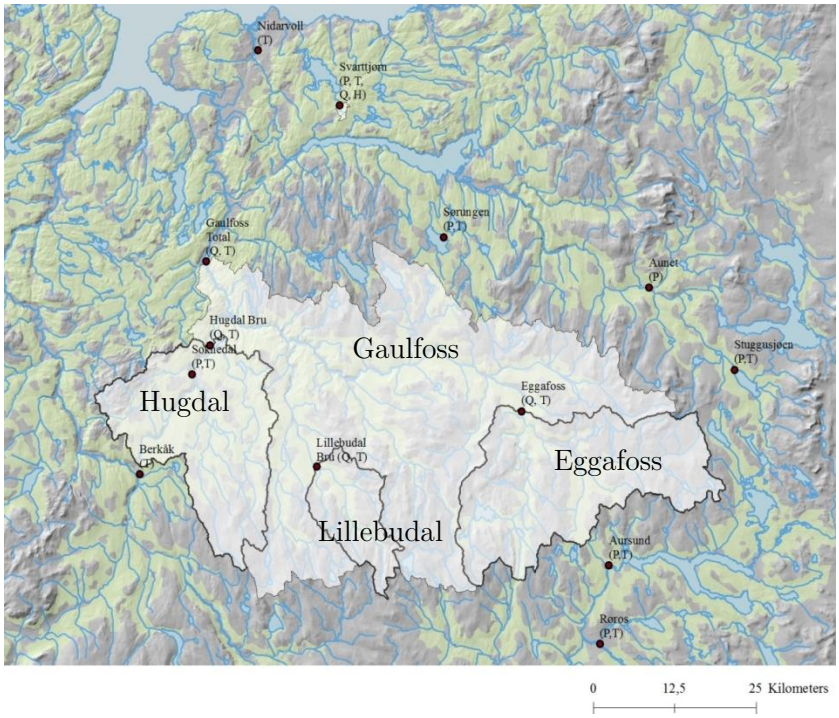

Figure 1. Overview of the study area. The letters after the station names refer to the data collected (Q = discharge, P = precipitation, T = temperature, H = humidity).

These facts are fundamental to evaluate the advantages introduced by the use of high resolution meteorological data, since in Svarttjørnbekken the density of the stations coupled with the small size of the catchment make the use of distributed inputs less effective than in Gaula, where ample spaces are left uncovered by meteorological stations and the choice of the interpolation method is more relevant. The two catchments are also different regarding the type of terrain: Svarttjørnbekken is completely forested and occupies an area with little slopes, while Gaula has both low elevation forested areas and also above the tree line expanses, especially in the southern parts. Generally, though, the region cannot be defined mountainous.

2.2 Distributed Geographical Inputs

2.2.1 Catchments

The catchments raster file is essential in order to specify the boundaries of each catchment by giving them an ID value that is necessary to aggregate the runoff from each cell of a catchment to produce the final runoff.

2.2.2 Digital Elevation Map (DEM)

Digital elevation maps are used in the ENKI model to be able to interpolate those variables that are correlated with the altitude (precipitation, temperature). The data was collected at 10m resolution from Statkraft's database and processed using ArcGIS, reducing the resolution by aggregating the cells with the "mean" method.

2.2.3 Forests Raster

A forest cover shape file was retrieved from Statkraft database and converted into a 1x1km raster file using ArcGis. The forest cover is used as it influences the shape of the snow depletion curve.

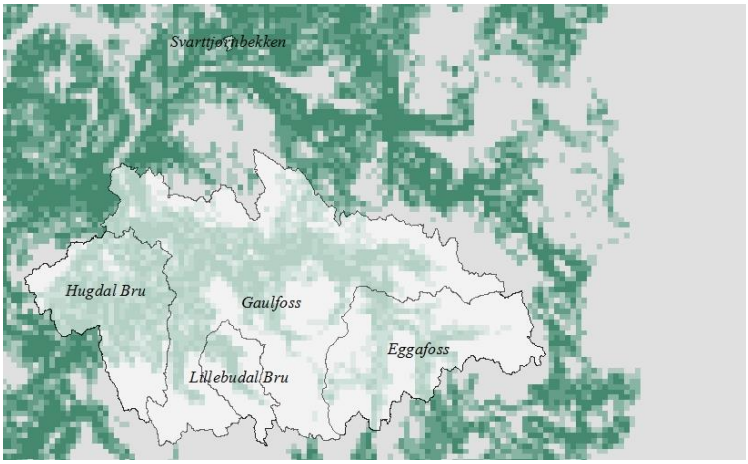

Figure 2. An example of a raster map, the forest cover. Green areas represent forested areas

2.2.4 Glaciers Raster

In the region there are no glaciers, so the relative raster (which is still required) will have a constant 0 value all over the region. Generally, glacier cover is represented with a number ranging from 0 to 100 in percentage representing the portion of each cell affected by a glacier.

2.2.5 Landuse

The landuse raster maps the presence of lakes. The model considers lakes as areas that produce instantaneously runoff from precipitation. In the considered region there are no big lakes that characterise the behaviour of the catchments.

2.3 Network Inputs

Relevant stations measuring precipitation, wind and temperature close to the two catchments have been used to retrieve the necessary data for the model.

The Svarttjørnbekken catchment is very small yet has precipitation, temperature, river flow and relative humidity coverage. On the other hand the Gaula catchment is much bigger and presents a lower density of measuring points; although there are 7 precipitation and 11 temperature stations in the surrounding areas, no observations represent the higher altitude mountains located in the southern stretches of the catchment, bordering the Forollhogna National Park. This is a condition that frequently happens, since stations are usually placed in locations with easier access, which usually happen to be in the valley and not in the mountains.

Station Name	Observations	Elevation [m.a.s.l.]	Xcoord*	Ycoord*
Gaulfoss Total	Q, T	50	562018	6998268
Lillebudal Bru	Q, T	520	579024	6966777
Hugdal Bru	Q, T	285	562623	6985385
Eggafoss	Q, T	420	610508	6975258
Røros	P, T	628	622503	6939642
Aursund	P, T	632	623904	6951638
Røstefoss	P, T	612	616620	6932790
Soknedal	P, T	299	559801	6980956
Aunet	P	302	630016	6994252
Stuggusjøen	P, T	627	643166	6981623
Sørungen	P, T	460	598466	7001933
Svarttjørn	P, T, Q	280	582558	7022170
Berkåk	T	475	551844	6965643
Helligdagshaugen	H	280	582364	7019879
Nidarvoll	T	44	570004	7030626

Table 1. Stations used in the model, along with their UTM32N coordinates and elevations.

2.3.1 Radiation Data

Due to the scarce availability and/or quality of the radiation data, in all the tests and calibration synthetic data has been used. Hourly values of extra-terrestrial incoming solar radiation were calculated using FAO's suggested equation, explained below:

$$\begin{cases} R_a = \dfrac{12(60)}{\pi} G_{sc} d_r [(\omega_2 - \omega_1)\sin(\varphi)\sin(\delta) + \cos(\varphi)\cos(\delta)(\sin(\omega_2) - \sin(\omega_1))] \\ d_r = 1 + 0.033\cos\left(\dfrac{2\pi}{365} J\right) \\ \delta = 0.409\sin\left(\dfrac{2\pi}{365} J - 1.39\right) \\ \omega_1 = \omega - \dfrac{\pi}{24} \\ \omega_2 = \omega + \dfrac{\pi}{24} \\ \omega = \dfrac{\pi}{12}[(1 + 0.06667(L_z - L_m) + S_c) - 12] \\ S_c = 0.1645\sin(2b) - 0.1255\cos(b) - 0.025\sin(b) \\ b = \dfrac{2\pi(J - 81)}{364} \end{cases}$$

where,

R_a	= extra-terrestrial radiation during the hour period	[MJm^{-2}hour^{-1}]
G_{sc}	= solar constant → 0.0820	[MJm^{-2}min^{-1}]
d_r	= inverse relative distance Earth-Sun	
J	= number of the day of the year	[1 to 365/366]
δ	= solar declination	[rad]
φ	= latitude	[rad]
ω_1	= solar time angle at beginning of the period	[rad]
ω_2	= solar time angle at the end of the period	[rad]
ω	= solar time angle at midpoint of hourly period	[rad]
L_z	= longitude of the centre of the local time zone	[° west of Greenwhich]
L_m	= longitude of the measurement site	[° west of Greenwhich]

2.3.2 Wind Data

Wind data is not available from stations that are close enough to be representative of the area. Thus a constant value of 2.5 m/s, found to be a good compromise from previous experiences, has been adopted.

2.3.3 Precipitation and Temperature Data

Temperature and precipitation data are widely available at measuring stations across Norway. Though, being precipitation and temperature the two most important inputs to every hydrological model, analysis of the data to assess its consistency is of extreme priority. Missing or suspicious data were deleted and the raster values were calculated with values coming from inverse distance weight interpolation (for precipitation, see Figure 3) or Bayesian Kriging (for temperature, see Figure 6) from the other nearby stations.

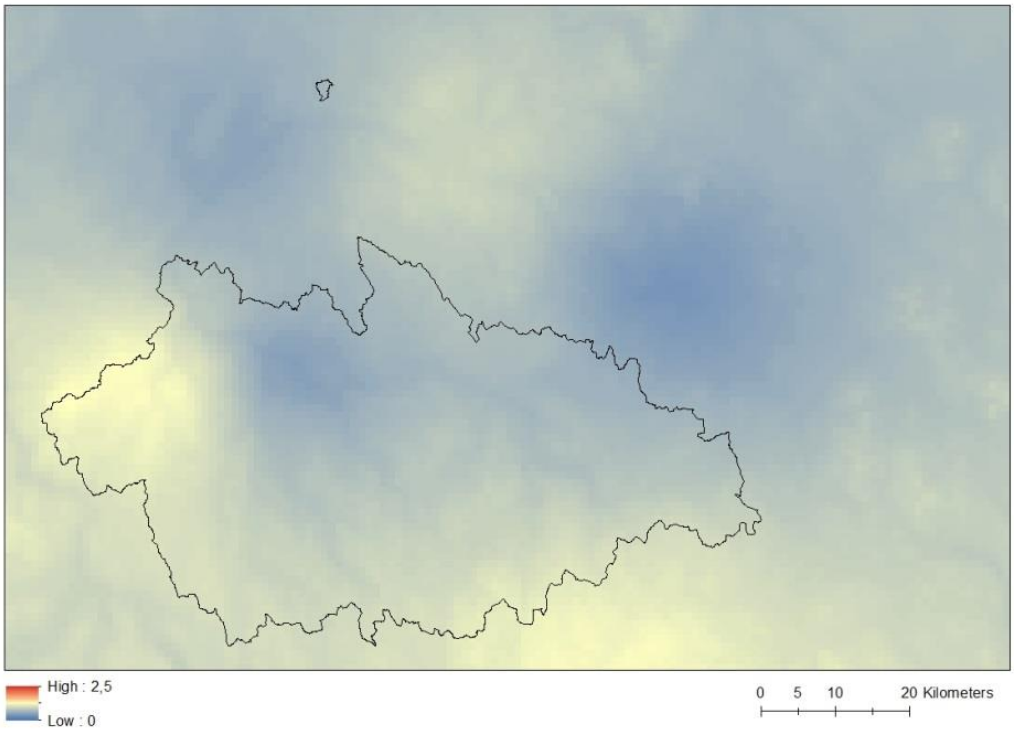

Figure 3. Example of IDW interpolation for precipitation observation for the 2nd March 2013.

A good way to estimate the reliability of the temperature and precipitation data is to compare the timeseries through accumulation plots, where trend in the observations (f.ex. sudden increase of average precipitation catch efficiency or measured temperature) become clearly visible.

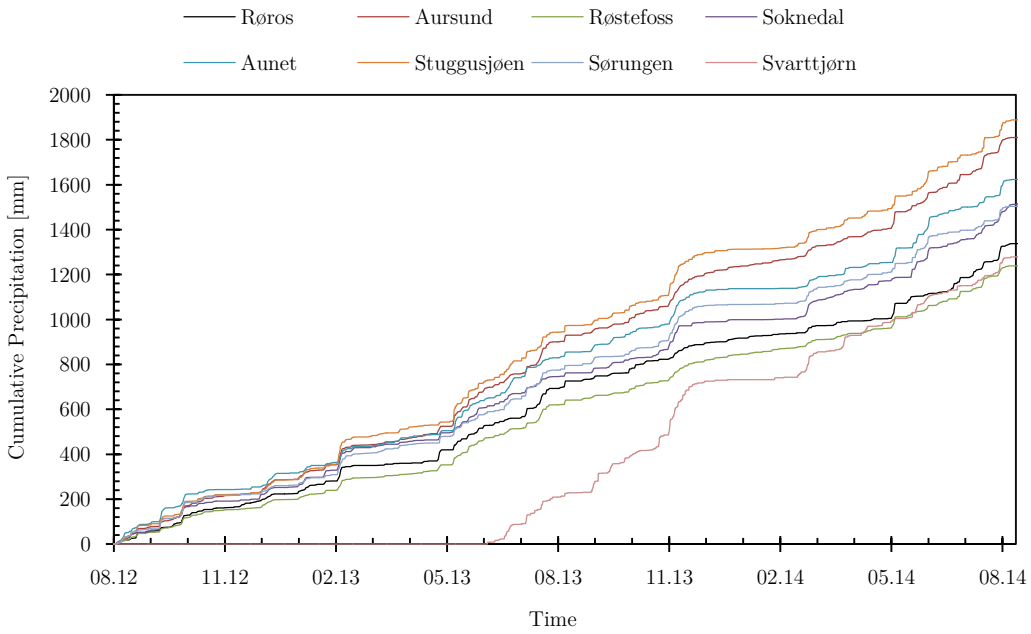

Figure 4. A plot of the cumulative precipitation for all the stations. Generally, with the exception of Svarttjørnbekken, the observations follow the same patterns.

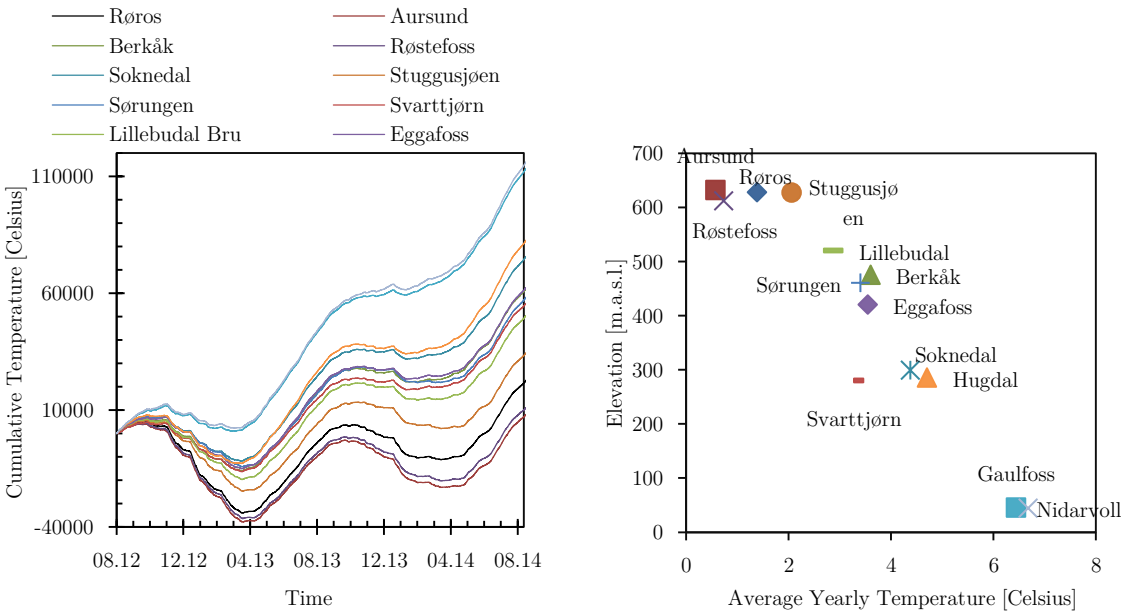

Figure 5. Cumulative temperature (left) and variations in annual mean temperatures with elevation.

Observing Figure 4 it is possible to notice that closeby stations generally follow the same patterns with some exceptions; Røros and Røstefoss values lye below the other curves, which is as aspected since they are located more inland in areas that receive less precipitation. Surprisingly, though, the Aursund station, only 12km north of Røros, shows a different behaviour with almost 40% more precipitation than Røros. Sørungen and Aunet, because of

their close distance, catch very similar amounts of precipitation: however, Stuggusjøen (18km south-est of Aunet) has around +18% in total precipitation, which is partially due to its higher elevation (+324m). Lastly, Svarttjørnbekken seems to be catching much more precipitation than the other stations, but no direct verification is possible since there are no other observations in the proximity to compare with. Precipitation data here starts from June 2013, thus for the preceding months data is interpolated from the closest stations automatically by ENKI. This probably degrades the simulation performance.

Regarding temperature measurements Figure 5 shows a consistent variation pattern that is mainly influenced by elevation: fitting a line with linear regression techniques gives an estimation of a temperature gradient of -0.97 °C/100m with $R^2 = 0.9$. From the above, no special problems can be spotted.

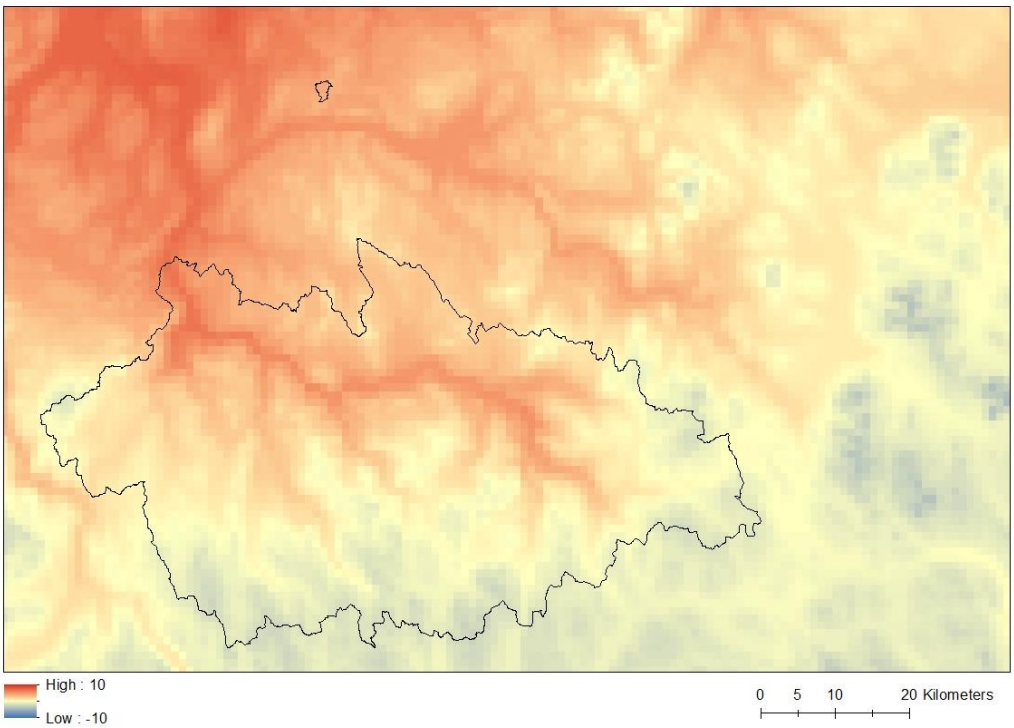

Figure 6. Output from the Bayes Kriging interpolation routine for the temperature for the 2nd March 2013.

2.3.4 Relative Humidity Data

Relative humidity data has been taken from one single available station in Svarttjørnbekken. The Gaula catchment is not covered by any humidity data and therefore a constant value of 80% is adopted.

2.3.5 River Discharge

Data regarding the hourly flow through sections of the unregulated rivers has been necessary in order to carry out a calibration of the parameters through the shuffled complex evolution algorithm.

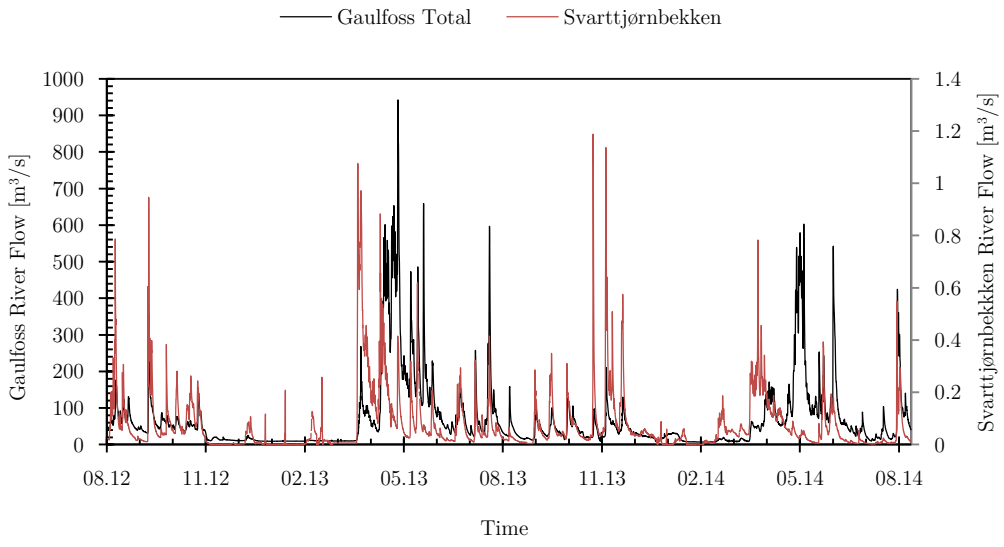

Figure 7. Observed river discharge for Gaula and Svarttjørnbekken

Since the evaluation of the model's parameters and, thus, its performance are strictly connected to the observed runoff for comparison purposes, it is of extreme importance that flow observations are consistent and correct. By only observing Figure 7 it is difficult to point out any potential error in the measurements. Such analysis will thus be covered during the discussion of the calibration results. What can be pointed out at this stage is the lack of a continuous timeseries for Svarttjørnbekken: during the 24 months analysed period, 105 hours are missing and data is not available or heavily lacking before summer 2012. This lowers the reliability of the time serie. Furthermore, the "Gaulfoss Total" data is the most downstream gauging station considered in the Gaula catchment and includes three gauged catchments (Lillebudal Bru, Hugdal Bru, Eggafoss): the difference between Gaulfoss total and the sum of the other three catchment gives the resultant "Gaulfoss Local". Though, negative flows are present in many periods, again highlighting the problem of the quality of the data, as shown in Figure 8, with negative figures down to -160 m^3/s.

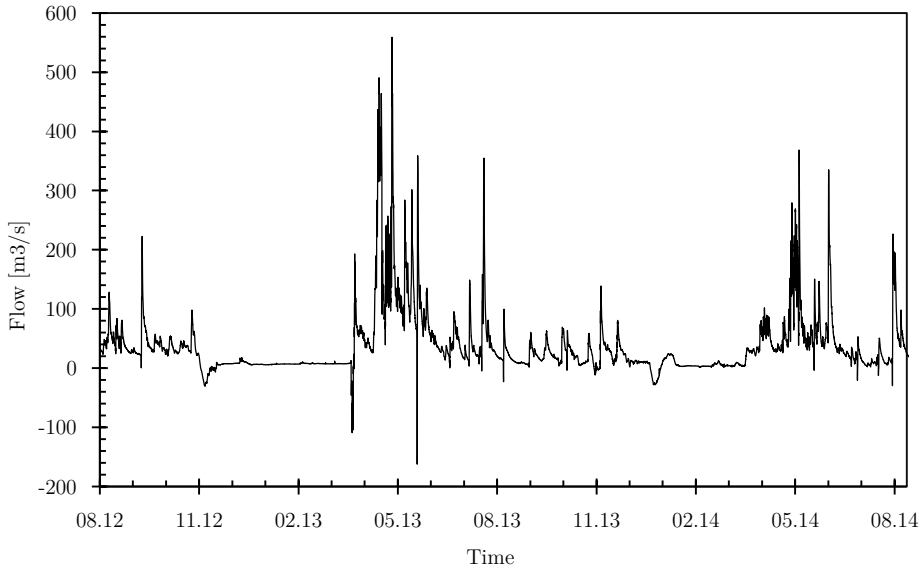

Figure 8. Resultant local Gaulfoss discharge and its negative values.

2.4 Distributed Meteorological Inputs

The Norwegian Meteorological Office is at present utilizing the modern AROME model to produce 2.5x2.5 Km forecasts. Updates are available every six hours and represent the most recent forecast runs of the meteorological models. Since there is not an actual data archive containing hourly "observation corrected" meteorological states, during the analyses the first 6 hours of each forecast were consider to represent the hourly observation for that timeframe.

The distributed rasters include data for precipitation, temperature, wind, cloud cover and relative humidity. These cover four of the five inputs necessary to ENKI. Radiation estimates could be simulated by using cloud cover data provided by DNMI and using empirical reduction factors for the incoming solar radiation. For the purpose of this thesis, such possibility has not been explored.

At this stage it is important to point out that the measurements from the precipitation stations are not used to update the initial conditions of the AROME model. The model is updated by assimilating other types of observations, such as satellite, vertical profiles captured by radiosondes, and ground stations reporting temperature and pressure. Temperature, precipitation, and wind are calculated by starting with the initial conditions and then numerically simulating forward in time the Navier-Stokes equations as well as thermodynamics equations. In addition, there are parameterization schemes that predict precipitation formation, short and longwave radiation effects, and surface interactions.

2.4.1 Data Processing

DNMI offers free download service for their AROME output forecasts; this data is updated every six hours and is stored in NetCDF files that cover a vast region including Norway, Sweden, Finland, and parts of the Baltic countries and Denmark. Since ENKI requires raster inputs with the same geometry and alignment as all the other distributed geographical inputs, it has been necessary to develop a code in Python that allows to automatically process the NetCDF file into a product that can be used by ENKI. The processing includes:

- Loading the NetCDF file
- Extracting the desired meteorological variables
- Reprojecting the extracted variables
- Clipping to region's geometry
- Resampling with bilinear interpolation to region's resolution
- Exporting to IDRISI raster file format (.rst)

Most of the steps above are performed using the GDAL library. Of the nearly fifteen thousand file that were processed, a part was missing or made up of wrong data.

Put a table showing missing days and bad data.

All in all, missing or wrong data composes 8.7 % (of which 53% is missing data) of the whole analysed period. This fact could certainly have a negative effect on the final results. To solve the problem, it has been decided to substitute these time step with raster files that were the final product of the interpolation run in ENKI using the network inputs. As shown in the discussion of each data type, this fixed the problem in a pretty seamless way, especially for temperature where the Bayes Kriging method produces results that are extremely similar to those from AROME. On the other hand, while precipitation is difficult to evaluate given the completely different nature of the interpolation methods used by AROME and the IDW, the wind measurements are probably the most affected by the problem: since to network measurements were used in the PIHM, a constant value of 2m/s is also substituting the data from AROME, creating an obvious disharmony in the data.

Once all the rasters were correctly created and every data hole filled, further manual processing involved the creation of a IDRISI raster group file (.rgf) to be loaded into ENKI as input raster series.

2.4.2 Precipitation

The precipitation outputs from the AROME model were the reason that started the idea of trying to run a hydrological model with distributed inputs. Precipitation, in fact, is a highly variable local phenomenon that depends on many factors such as distance from the coastline, elevation, local morphology of the terrain etc. Because of these, the results produced by interpolating local observation are often poor and little representative of the

actual situation. IDW tends to produce circles of similar values around each stations, making the rasters look like full of clusters. Also the precipitation gradient is a poor measurement of the increased rainfall patterns with elevation, since it doesn't account for local effects such as direction of the prevailing wind and cloud system in a region, which affect, among the others, the side of a slope at which precipitation occurs due to the orographical effects.

Considering the results from the DIHM calibration (Chapter 3.6) and in particular the values (0.7-0.8) of the snow and rain correction parameters, which govern the water mass balance, it is evident that the model tries to adapt to the AROME data by scaling down the observed precipitation. This is highlighted also in the graphs below, where it is clear from the cumulative plots that AROME reproduces more precipitation than the observations suggest.

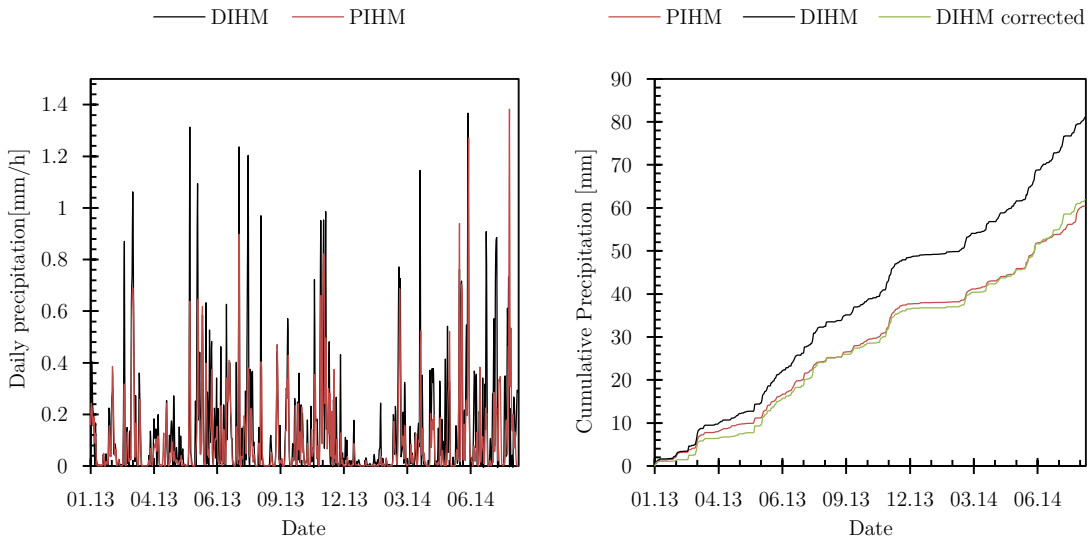

Figure 9. (left) Time series representing the average precipitation of the Gaulfoss catchment over the simulation period and (right) cumulative precipitation with attempted correction.

Two main considerations can be drawn by observing Figure 9. First of all, AROME data presents higher intensity precipitation that occurs more frequently than in the PHIM; the second consideration can be made by observing the right cumulative plots: the pattern and the forms of the curves are matching, which means that there is a good agreement between the observed and interpolated data and AROME. The main difference is, as said before, the amount of precipitation that is simulated. This could be a problem of scaling down the AROME data, or there could be a constantly occurring bias that is affecting the results. Observing the timeseries, it is noticeable that AROME almost never simulates a precipitation of 0mm/h, instead always gives small numbers. This little amount of precipitation could make a difference if summed during a long time frame. To test the significance of this observation, a filtering method has been applied by equalling to 0 all the

values that were below the 0.9 percentile value of 0.4mm/h. The result is the bias corrected DIHM, which is now very close both in shape and in the total amount of simulated precipitation. Of course, this doesn't solve the problem of the higher intensity of the precipitation, rather just cuts out less significant events. This only represents a test that has not been considered in the calibration and simulations of the model and is done only to show that further investigations are necessary in order to provide a better representation of the actual precipitation.

The advantages of having a more accurate AROME model rather than IDW interpolated observations lies in the fact that it has a better representation of the precipitation patterns, as it models the clouds systems and where a precipitation event is to be expected (see Figure 10 below, as compared with Figure 3).

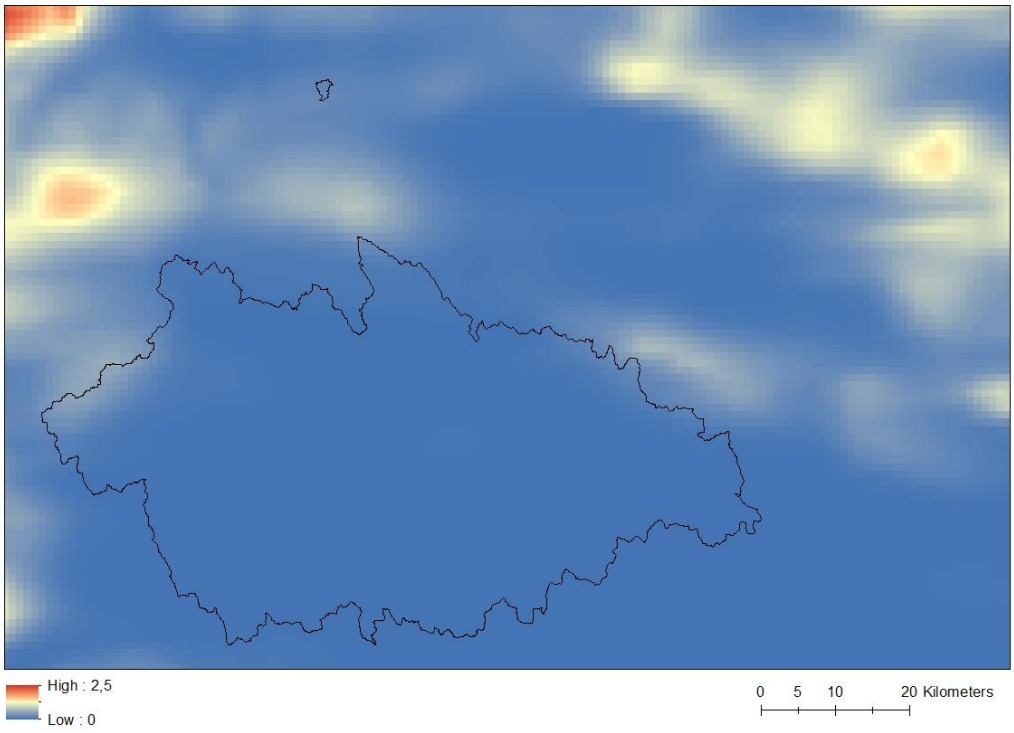

Figure 10. An example of AROME's precipitation raster, as simulated for the 2nd March 2013. Cloud systems are represented and precipitation acquires a more local connotation.

2.4.3 Temperature

If compared to the precipitation comparisons in the previous Chapter 2.4.2, surely temperature data shows a higher level of correlation between the outputs from the Kriking routine using network observations and the outputs from AROME model. Figure 11 shows a comparison between the average daily temperatures in the Gaulfoss and Svarttjørnbekken catcments. A close similarity is to be observed for both catchments, especially in the summer months. Some difference appear in the winter months, where the AROME model used in the PIHM model show higher temperatures for both winters and for both catchments as easily observable from the cumulative plots. Looking closer at the

temperature time series of the same Figure, it is noticeable how this is caused by lower low temperatures simulated by PHIM as opposed to DIHM, where the peaks are more smoothened out: warmer winter days are simulated by both models almost exactly in the same way, but more problems arise during the coldest winter days. A reason could be the difficulties in handling day-night temperature differences or days with temperature inversion, which is a hard to model meteorological phenomenon that refers to the reversal of the usual decreasing temperature gradient in the troposphere. Such events usually take place in restricted areas.

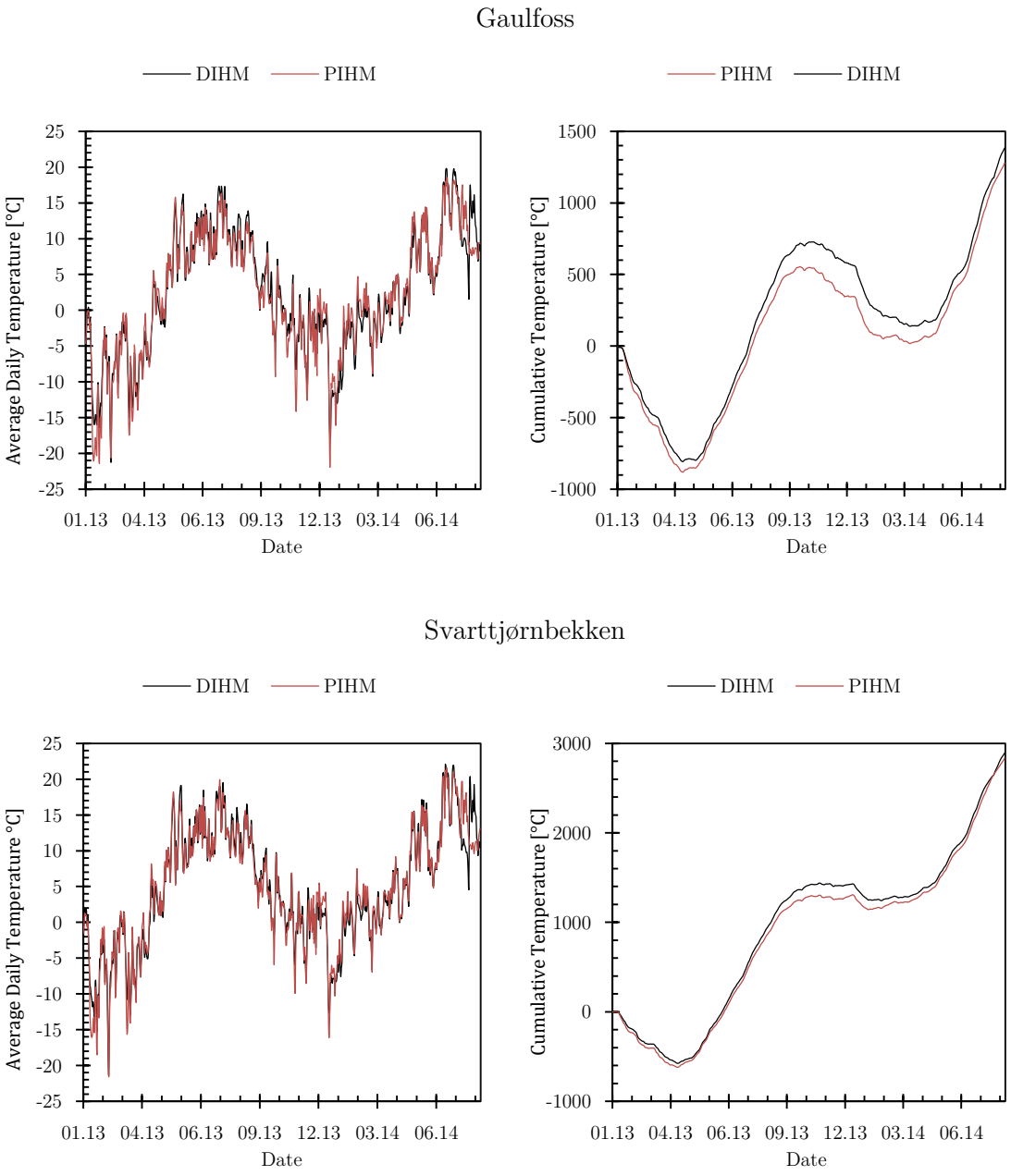

Figure 11. Temperature time series (left) of average daily temperatures and cumulative daily temperatures (right) for Gaulfoss (top) and Svarttjørnbekken (bottom)

Figure 12 shows an image representing the temperature simulated by the AROME model. Comparing it with Figure 6 shows a close correspondence in the results. The main noticeable difference is the higher spatial effective resolution; the word "effective resolution" refers to the fact that the AROME rasters has an actual native definition of 2.5x2.5km, but needs to be resampled in order for ENKI to run with them. Thus, though the final resolution of both images is 1x1km, the product of the Bayesian kriging shows finer details. AROME outputs with spatial resolution of half a kilometer are also available for download, but have not been used in this thesis. The correlation between the two methodologies is good enough to believe that the data used is good enough to provide high quality results. If a better hydrological simulation has to be achieved, it would be wiser to consider other factors than the temperature data.

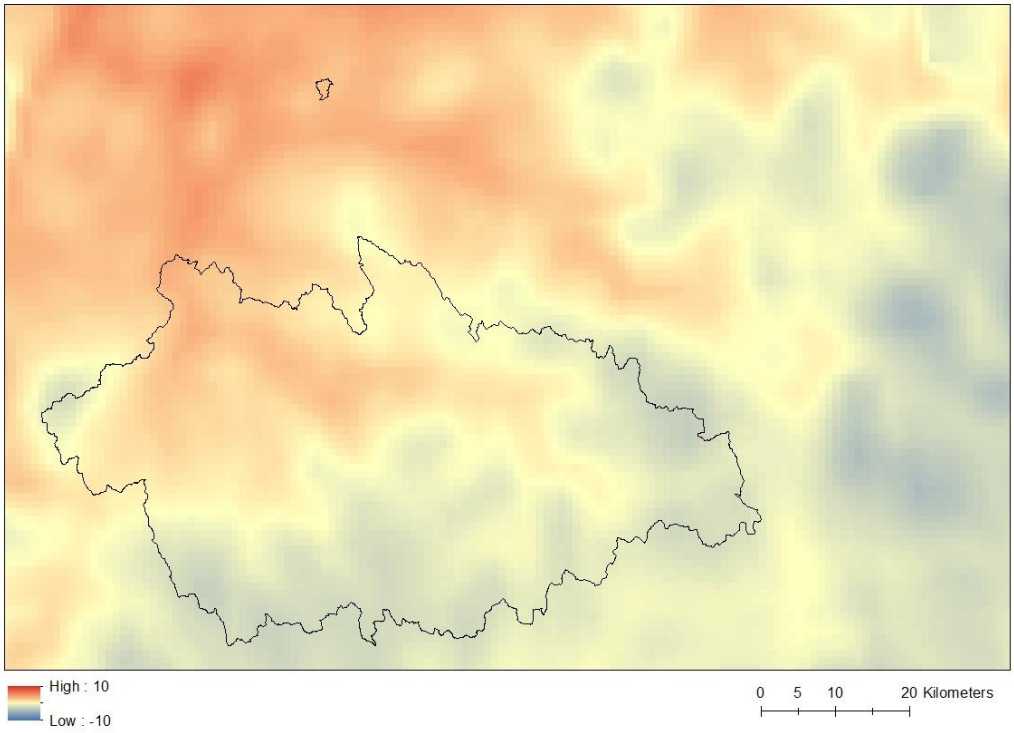

Figure 12. AROME temperature input for the 2nd March 2013. If compared to the interpolation from the Bayesian Kriging interpolation routine (see Chapter) the results show a high level of similarity.

2.4.4 Wind

The wind is a key parameter in the snow routine. From the meteorological data wind refers to 10m elevation, which is the normal height in this field as it tries to avoid problems connected with obstacles surrounding the station that might decrease the wind speed. To convert this values to the standard 2m elevation used for evaporation and snow routines, a logarithmic profile (see Figure 13) has been taken into consideration while adopting the coefficients suggested by FAO. Thus, a coefficient of 0.75 has been selected to scale the wind distributed inputs.

It is also important no note that wind speed reduction within a forest due to tree cover has not been taken into consideration. This probably causes an over-estimation of the simulated wind speed in a big portion of Gaula and Svarttjørnbekken.

A representation of spatially averaged values of the AROME wind data is shown in Figure 13. Gaulfoss correctly shows higher simulated values, since it includes mountainous areas where winds are generally higher. Some periods of missing AROME data were filled using the constant value of 2m/s as used in the PIHM model (and shown with a green line in Figure 13).

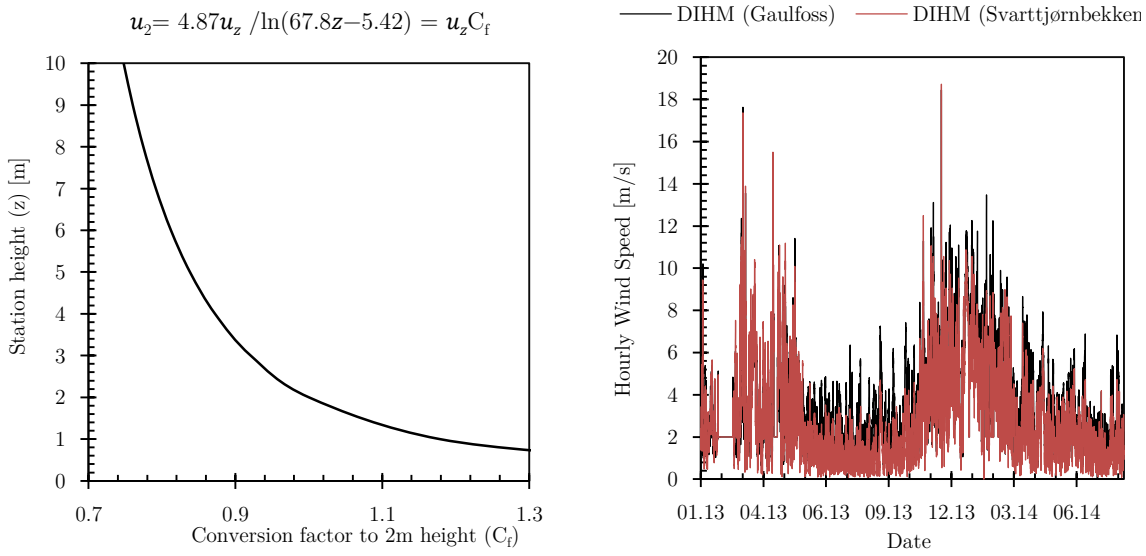

Figure 13. (left) Coefficient (C_f) to transform a 10m height wind measure (u_z) into the standard 2m and its equation. (right) Average hourly windspeed for Gaulfoss and Svarttjørnbekken catchments.

Chapter 3

Models Setups and Performances

3.1 ENKI

ENKI is an open source framework for running distributed models. The software was developed to be used within the hydrological field by SINTEF and Statkraft.

The main characteristic that made ENKI the ideal tool for this thesis work is its flexibility and adaptability: the model can be custom modified to include the desired routines and methods. For each one of these, there is the possibility to include modification or add new ones through C++ programming. This feature has been the basis that enabled the whole thesis work.

ENKI is structured to divide a setup in two parts: the region and the model. The region contains all the distributed inputs and informations (see Chapter 2.2), as well as stations' coordinates and parameter values. The model is made up by a stack of routines that are needed to transform the observed (or forecasted) inputs into the inflow. The routines are made up of parameters that link to the corresponding values stored in the region. Furthermore, other two components are the input and output databases, containing, respectively the values of the observations from the timeseries and the simulated variables, which can be also others than the inflow.

Calibration is made possible by a set of algorithms to choose from: the SCE-UA method has been selected as it is robust and has proven its reliability in many studies.

3.2 Model Structure

The structure adopted tries to deliver an alternative to the widely used and more common HBV model, by adopting more modern routines that have a higher degree of simulation performance while keeping down the total amount of calibration parameters: this restricts their freedom in the calibration which in turns delivers more stable and consistent parameters.

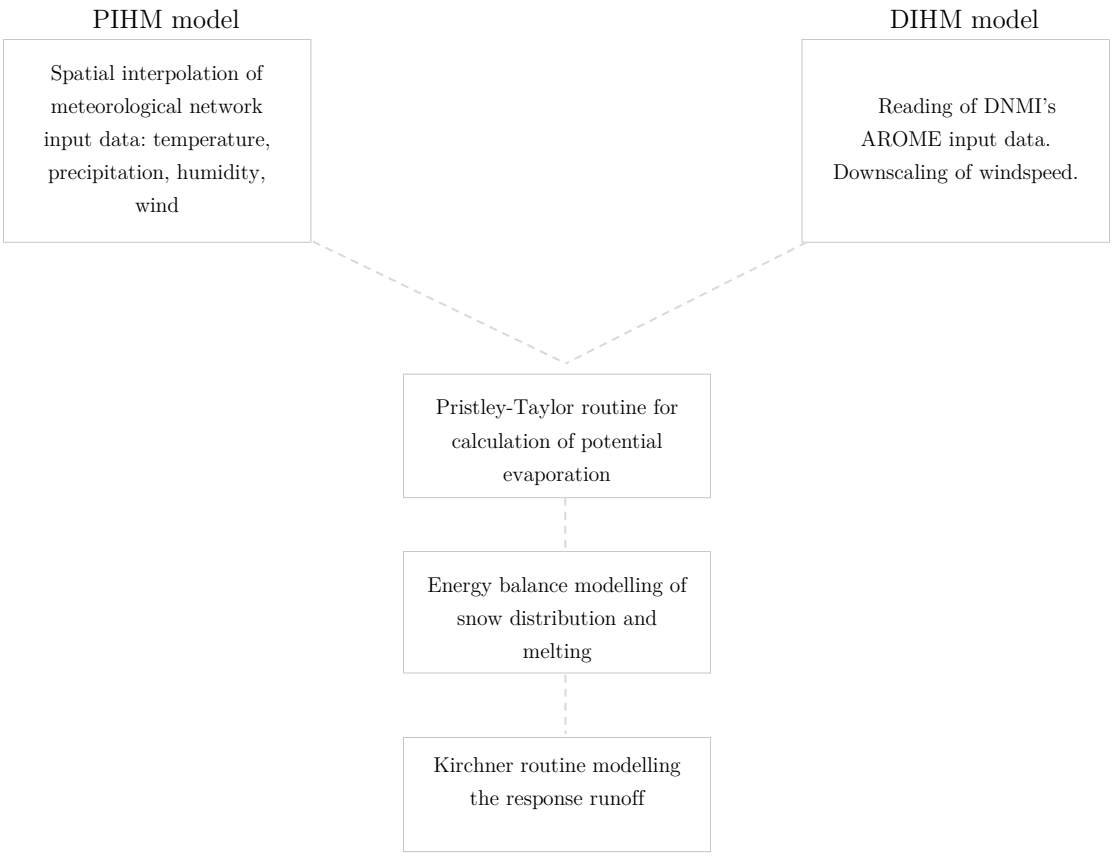

Figure 14. Schematic representation of PIHM and DIHM model stacks.

The general layout of the model can be represented as a four steps process:

- Interpolation and processing of meteorological input data (for PIHM only)
- Calculation of the potential evapotranspiration
- Snow energy balance modelling
- Response routine

3.2.1 Interpolation Routines

The interpolation of the point measurement in the PIHM model is done through inverse distance weight (IDW) for precipitation, wind and humidity and Bayesian Kriging for temperature. A precipitation gradient of 2.5%/100m was applied. For temperature, the Krigin routine estimated the gradient itself, thus not requiring any fixed value.

3.2.2 Priestley-Taylor Evapotranspiration Equation

For the estimation of the potential evapotranspiration the radiation-based Priestley-Taylor equation (Pristley & Taylor, 1972) has been adopted. This routine represents a simplification of the Penman-Monteith model which is largely used in areas with little to no

average water deficit. Its adequacy has been extensively tested in many papers [(Shuttelworth & Calder, 1979), (Stagnitti, Parlange, & Rose, 1989), (Weiss & Menzel, 2008)] where it has shown its reliability and consistency.

$$ET = 1.26\left(\frac{\Delta}{\Delta + \gamma}\right)(R_n - G)$$

where,

ET	= evapotranspiration	[mm/hour]
R_n	= net radiation	[mm/hour]
G	= soil heat flux	[mm/hour]
γ	= psychrometric constant	[kPa/°C]
Δ	= gradient of saturated vapour pressure	[kPa/°C]

3.2.3 Energy Balance Snow Routine

The GamSnow routine is an energy balance model that as main outputs gives the snow water equivalent (SWE) in each gridcell and its relative snow covered area (SCA). Since the spatial resolution of the model doesn't allow to distinguish between different snow depth distribution given mainly by topographical factors, SCA is a necessary variable that represents the spreading of the snow. SWE and SCA are linked together by the snow depletion curve. Depletion curves relate the snow covered area to the cumulative snow melt from an arbitrary day considered the end of winter.

From these two variables, the melt runoff can be calculated.

Generally, it represents a more data intensive model than the common "Degree Day" models.

The routine uses a simplified version of the more complex and generic energy balance equation:

$$\frac{\Delta U}{\Delta t} = Q_{sn} + Q_{li} + Q_p + Q_g + Q_{le} + Q_h + Q_e + Q_m.$$

Where ΔU is the variation in the energy content during the Δt time step, Qsn represents the net shortwave radiation, Qli the incoming shortwave radiation, Qp the heat from precipitation that falls on the snow pack, Qg the flux of heat from the ground beneath, Qle the outgoing longwave radiation, Qh the sensible heat flux, Qe the latent heat exchanges and finally Qm is the heat removed by metltwater.

3.2.4 Response Routine

The response routine is modelled using Kirchner's methodology, which is described more in depth in chapter 3.4. It has shown its incredible strength due to its simulation performance, low number of parameters and the possibility to estimate their values by

analysing the hydrograph. Thus, potentially, for catchments with a good quality of hourly inflow and meteorological data, the Kirchner's response routine does not require to calibrate any parameter.

3.3 Parameter Calibration

3.3.1 Calibration Parameters

For the reasons further explained in Chapter 3.8, during the calibration phase one of the main focuses has been to keep as low as possible the number of parameters: the computational effort required to calibrate on hourly timestep couldn't allow for many thousand runs, thus a more restricted parameter set is more easily definable. Furthermore, this would help improving the consistency of the variables by reducing inter-dependence and compensation which could hinder forecasting performance.

The choice of calibration parameters was suggested by previous experiences about which ones are the most determinant in the simulation process.

The following seven parameters where selected:

1. PcorrRain : correction factor for the rain catching efficiency at the measuring station
2. PcorrSnow : correction factor for the snow catching efficiency at the measuring station
3. Tx : temperature limit to distinguish between rain and snow
4. Windscale : slope of the turbulent wind function, governing heat exchanges
5. Rscale : radiation scaling factor, to take into account average cloud cover and slopes
6. lnTau3 : response coefficient, governing the base speed of the response
7. dlnTaudlnQ : response coefficient, controls the speed of response at varying flow levels

Of these, the first two are slightly redundant variables governing water balance. Another option would have been to incorporate the precipitation gradient variable, but from previous test it was possible to see that this possibility was creating too much compensation between the three parameters, suggesting that there is no need to include them all.

Tx and Windscale are mainly influencing the snow routine; Tx could be also considered a water balance "by type" variable since it distinguishes precipitation between rain and snow. Windscale has been found to be of high importance for the snow routine since it governs the sensible and latent heat exchanges, which are influenced by the presence of wind.

3.3.2 Objective Function

The objective function, used to evaluate the performance of the hydrological model and for calibration purposes, is the "Nash-Sutcliffe model efficiency coefficient" (Nash & Sutcliffe, 1970) defined as:

$$E = 1 - \frac{\sum_{t=1}^{T}(Q_o^t - Q_m^t)^2}{\sum_{t=1}^{T}(Q_o^t - \overline{Q_o})^2}$$

where T is the total number of time steps, Q_o^t and Q_m^t are respectively the observed and modelled discharges at time step t, and $\overline{Q_o}$ is the average observed discharge. The nature of this coefficient tends to give a much greater importance to high flows since their relative error is higher. This could cause the calibration process to pick values that perform well for the melting season but that are not suited for the rest of the year when the flows are lows (for example in winter). Thus, for the purpose if this work, also the natural logarithm of the Nash-Sutcliffe coefficient has been taken into account to give more weight to low flows.

3.3.3 Calibration Algorithm

Many possible methodologies are widely available in the literature, but in this thesis only the Shuffled Complex Evolution from the University of Arizona SCE-UA (Duan, Sorooshian, & Gupta, 1992) calibration algorithm has been used. SCE-UA represents a global search algorithm that optimizes an objective function by looking at the whole parameters space shuffling random samplings.

3.4 The Kirchner's Routine

The KirchnerMod routine in ENKI has been developed by Sjur Kolberg at SINTEF starting from the paper "*Catchments as simple dynamical systems: Catchment characterization, rainfall-runoff modeling, and doing hydrology backward*". (J.W.Kirchner, 2009)

It consists in a response routine that is made up of three calibration parameters (evapQscale, lnTau3, dlnTaudlnQ), three distributed inputs (outflow from snow routine, potential evaporation and fractional snow covered area) and one single state (instantaneous runoff), see Figure 15.

Figure 15. Schematic representation of the Kirchner Routine inputs, outputs and states.

Kirchner's analysis starts with the conservation of mass equation,

$$\frac{dS}{dt} = P - E - Q$$

where P, E and Q are precipitation, actual evaporation and runoff per unit of time.

Assuming that the discharge Q only depends on the water storage (S) in the catchment (thus not considering direct precipitation into the river and onto impermeable or saturated zones) with a monotonically increasing function, we end up with an invertible relation:

$$Q = f(S) \ and \ \ \frac{dQ}{dS} > 0 \ \ \forall Q,S \implies S = f^{-1}(Q)$$

The important and logical consequence of this assumption is that, being Q only a function of S, the discharge will increase whenever (P – E) > Q and vice versa.

Furthermore, the model is "flexible" and doesn't restrict the function to have any particular form.

Combining the first two equations then yields,

$$\frac{dQ}{dt} = \frac{dQ}{dS}\frac{dS}{dt} = \frac{dQ}{dS}(P - E - Q) \implies \frac{dQ}{dS} = \frac{\frac{dQ}{dt}}{(P - E - Q)}$$

Thus the Q-S relationship can be found depending on the rate of change of the discharge and the "instantaneous" measurements of precipitation, evapotranspiration and water flow.

Of these, three can be acquired through meteorological stations, but only the Q measurement is really a value that describes the catchment as a whole, since P and E are taken at a point and are affected by high spatial variability.

Therefore, for those time-steps where $P,E \ll Q$, it is possible to write

$$g(Q) = \frac{dQ}{dS} \approx \left.\frac{-dQ/dt}{Q}\right|_{P,E \ll Q}$$

This implied that the Q-S can be estimated only using observations of the river flow.

It is then possible to calculate the storage-discharge relationship by integration.

$$\int dS = \int \frac{dQ}{g(Q)}$$

3.4.1 A Priori Estimation of the Kirchner's Parameters

In order to estimate the storage-discharge relationship solely from observation of the river discharge, it is necessary to isolate those timesteps where precipitation and evapotranspiration are negligible compared to the flow.

One of the suggested methods in the paper is to proceed with the analysis of hourly data and detect the timesteps where no precipitation is present in the catchment and where relative humidity is close to 100%, i.e. when there is little evaporation. To do this, only rainless night hours are considered, assuming that during the dark hours of the day the evaporation is negligible both because of the absence of solar radiation and because of the higher humidity generally present at night. Night hours are identified as those with an average solar radiation of less than 1 W/m^2.

It is then possible to plot the flow recession rate $-dQ/dt \approx (Q_{t-\Delta t} - Q_t)/\Delta t$ as a function of discharge $Q \approx (Q_{t-\Delta t} + Q_t)/2$, as shown in Figure 16. Here the lack of observed and analysed data didn't allow to follow the procedure described by Kirchner of creating a linear regression from a plot with binned averages.

In order to give more weight to low values Kirchner suggests to transform the points into their natural logarithms. At low values of Q, some points might have negative values, and is therefore necessary to solve the problem by binning them into ranges of Q. This should be done in a way that the intervals include enough points that the standard error of –dQ/dt within each bin is less than half of its mean.

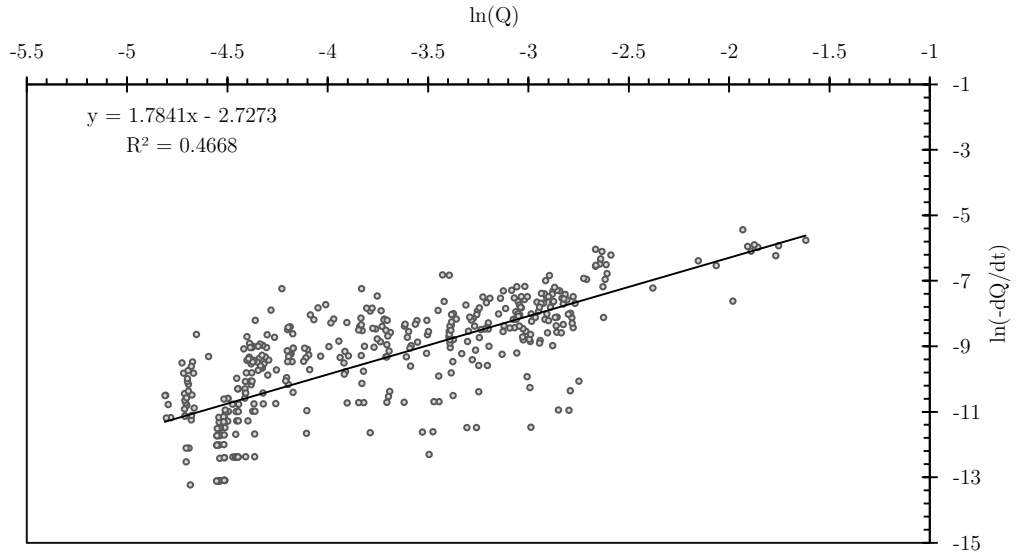

Figure 16. Flow recession plot in a logarithmic view and its linear interpolation.

Once a linear regression is fit into the natural logarithm plot of the binned averages points, it is possible to obtain the relationship

$$\ln\left(-\frac{dQ}{dt}\right) = a\ln(Q) + b$$

Since we are interested in solving the integral described in chapter 3.4,

$$\ln\big(g(Q)\big) = \ln\left(\frac{-\frac{dQ}{dt}}{Q}\right) = \ln\left(-\frac{dQ}{dt}\right) - \ln(Q) = (a-1)\ln(Q) + b$$

Now that the form of g(Q) is known, the integral can be solved.

Kirchner equation then represent a simple response model based on only two parameters, a and b. These two values can be used in ENKI in the KirchnerMod routine after being converted to *lnTau* and *dlnTaudlnQ*.

LnTau3 represents the value of ln(g(Q)) when ln(Q) = 3, while is *dlnTaudlnQ* = (*a*-1).

3.5 PIHM Calibration Performance

Seven parameters (see Chapter 3.3) were calibrated in the Point Inputs Hydrological Model.

The results show different performances across the calibration catchments, and this Chapter is intended to give an analysis of their causes.

Catchment	R^2	$\ln R^2$
Gaulfoss	0.80	0.78
Lillebudal Bru	0.53	0.36
Hugdal Bru	0.59	0.64
Eggafoss	0.83	0.75
Svarttjørnbekken	0.50	0.57

Table 2. R2 performances of the PIHM model with all available stations

The Figure 17 shows a very good match between the simulated and observed discharges both in the high flows and in the low flows for the Gaulfoss catchment. However for Svarttjønnbekken the low R^2 performance value is probably to be explained by the missed high flows in June and November 2013; this can be either caused by missed precipitation events, by an unmodelled snow melts (unlikely in the June event) or simply an error in the measurements. A part from this event, the model produces satisfying results.

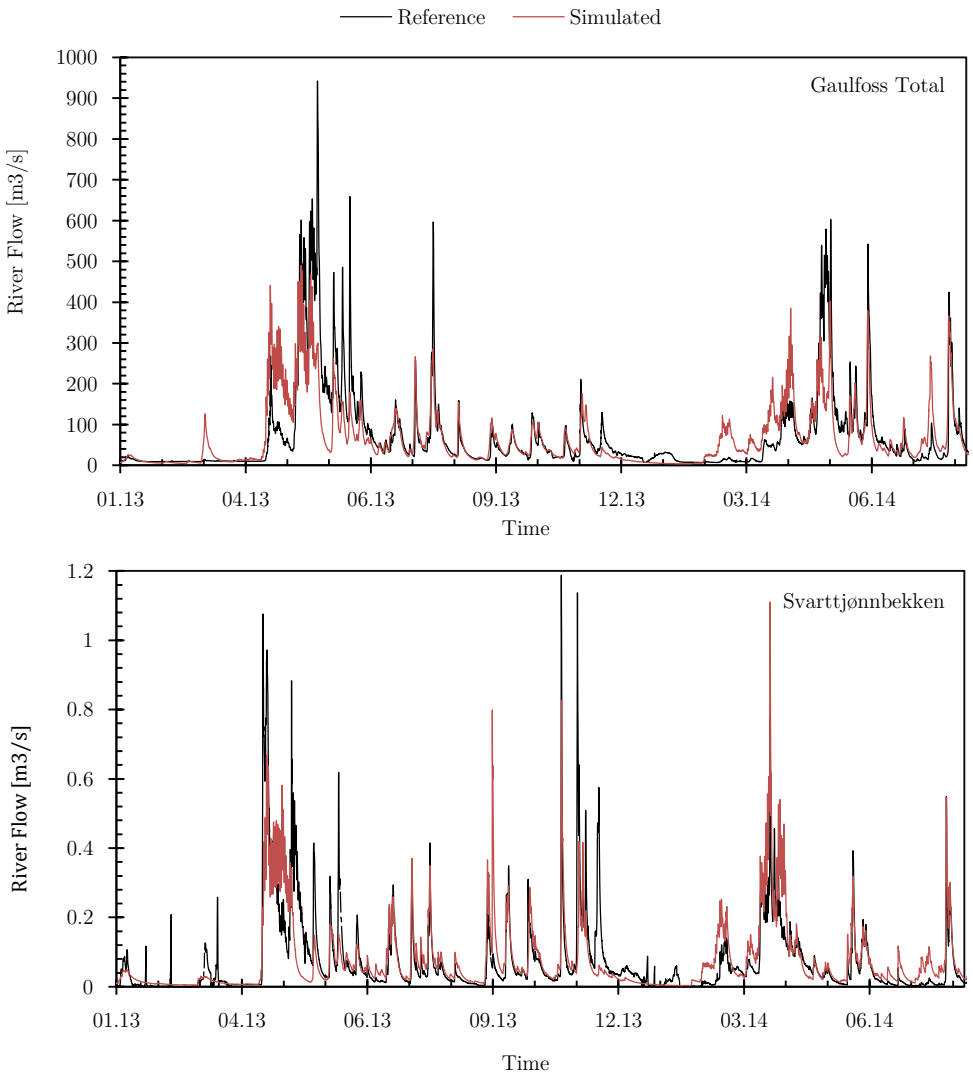

Figure 17. Simulated and Observed Runoffs for the PIHM model with all stations included.

At this point, it is important to highlight once again that for calibration purposes one year and a half of data is not enough to set up a model that can be representative of a catchment under many varying conditions (prolonged low flows, high floods, sudden snow melts, particularly high precipitations etc.). Since the purpose of this chapter is to describe the quality of the PIHM and DIHM simulations, in order to make comparable and fair results, another calibration has been run including in the input network only those stations that are used by the meteorological model, i.e. DNMI's own stations. The results change slightly, as shown in Figure 18 and it is mainly due to missed peak flows and less precise low flow condition. In particular the two high flow events in Svarttjønnbekken that were missed in the previous test case, are accentuated here further; a higher release of water earlier in April 2013 lowers the availability to cover the unmodelled event. Furthermore the ability to reproduce fast peak runoffs is reduced. On the other hand, spring melt events seem to be better simulated by the second test. Of interest it is to point out the difference, in both test cases, found in the response parameters for Gaulfoss and Svarttjørnbekken: the first has

from calibration a lnTau3 value of 5.87 against the 4.9 of the second (lower values mean faster response); this probably reflects the fact that being Gaulfoss a much bigger catchment, this parameter is including in itself all the delays and routings that happen during the time it takes for the flow produced by each cell to reach the measuring pint. Therefore it is safe to assume that even if no direct routing routine has been implemented yet in ENKI, the response parameters are somehow taking care of these effects.

Catchment	R^2	lnR^2
Gaulfoss	0.77	0.79
Lillebudal Bru	0.49	0.51
Hugdal Bru	0.56	0.67
Eggafoss	0.85	0.74
Svarttjørnbekken	0.44	0.56

Table 3. Nash-Sutcliffe coefficients for the five catchment using only DNMI's stations

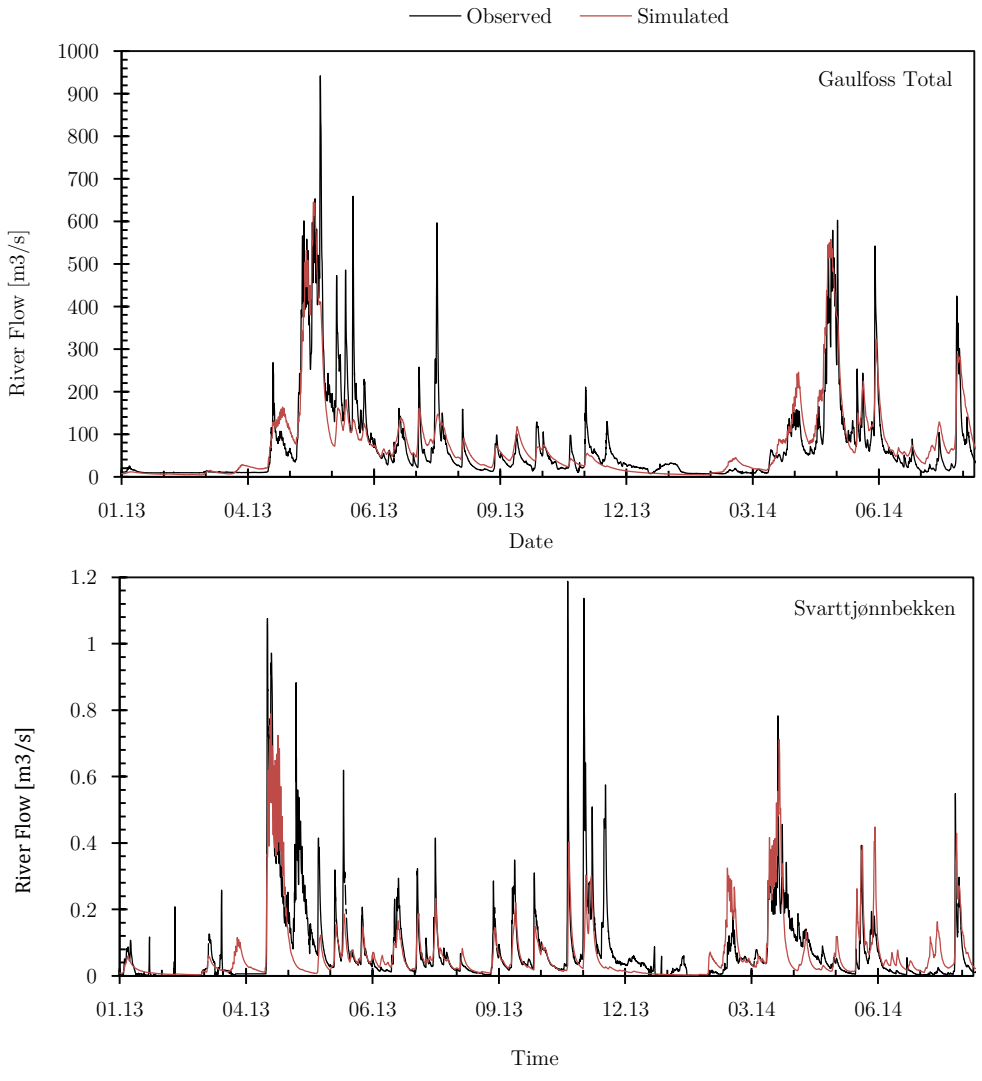

Figure 18. Flow simulation without Statkraft's and NVE's stations.

3.5.1 Parameters Sensitivity

Seven parameters were calibrated in PIHM (see Chapter 3.3.1).

From previous experiences Tx, Windscale and lnTau3 are among the parameters that most influence the model performance. Parameter sensitivity analysis and their stability/definability are important in order to have a consistent model with stable and defined parameters.

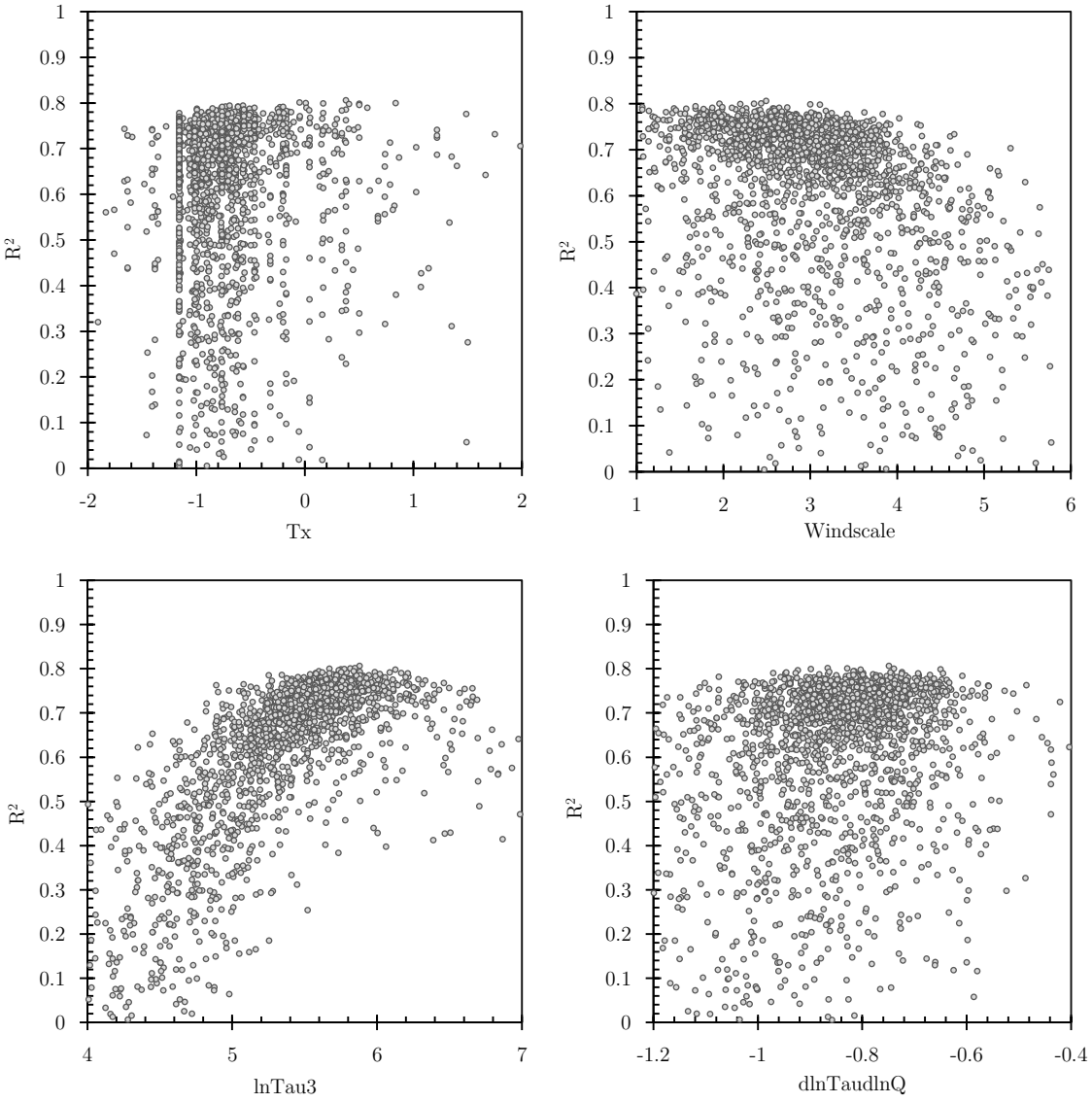

Figure 19. Parameter sensitivity analysis for Gaulfoss: only lnTau3 has a clear value that achieves the best model performance. For the other three variables, only a more general optimal area can be identified.

This is especially important in the process of regionalisation, where the values of the variables are associated with catchment properties. In practice, though, the lack of a real physical representation of the model makes the parameters be an aggregated measure of various processes that are described only conceptually and generically; this limits the

possibilities of regionalisation and of finding obviously representative parameters. The higher the degree of inter-compensation the harder it is to get defined variables from the calibration.

Figure 19 shows that only lnTau3 has a clearly defined maximum (5.77 from calibration), while the others only have an optimal zone that can be identified. This, as mentioned, is a problem with conceptual models and increases the uncertainty related to the choice of correct and stable parameters through time. For this work a validation period is not considered for the models, even though it is generally good practice to test a setup during another timeframe, thus the parameters will be taken as suggested by the calibration process.

3.6 DIHM Calibration Performance

The main purpose of calibrating with distributed data from the AROME model is to verify its reliability and quality, especially concerning the precipitation data. In order to test the advantages and contribution of each dataset, first a model including only the temperature and precipitation inputs has been included. Afterwards, the wind data has been added to see if the simulations could be further improved by substituting the constant wind parameter of 2m/s with modelled windspeeds. During these tests, the parameter controlling actual evaporation has been calibrated instead of the radiation scaler in order to adjust it to the different precipitation type of AROME, showing in general higher rainfall patterns.

The calibration results with the temperature and precipitation only inputs showed in general a lower performance (see Table 4). Moreover, and surprisingly, the performance of the DIHM model including wind simulations performed equally as the PIHM model that only consideres DNMI's stations. There is thus a good base to believe that if DNMI's AROME model also included Statkraft's and NVE's stations, a further improvement good be achieved.

	T+P		T+P+W		TPW - PIHM	
	R2	lnR2	R2	lnR2	R2	lnR2
Gaulfoss Total	0.73	0.73	0.75	0.76	-0.02	-0.03
Lillebudal Bru	0.52	0.32	0.55	0.49	+0.06	-0.02
Hugdal Bru	0.52	0.62	0.53	0.64	-0.03	-0.03
Eggafoss	0.77	0.70	0.80	0.75	-0.05	+0.01
Svarttjørnbekken	0.51	0.51	0.54	0.52	+0.10	-0.04
					+0.01	-0.02

Table 4. Comparison of simulation performances between two different distributed model setups and the model with observation inputs (T=temperature, P=precipitation,W=wind)

The plots showing the simulaitons with the model including wind data are visible in Figure 20. The results are very close to what was obtained with the PIHM method including only DNMI's stations.

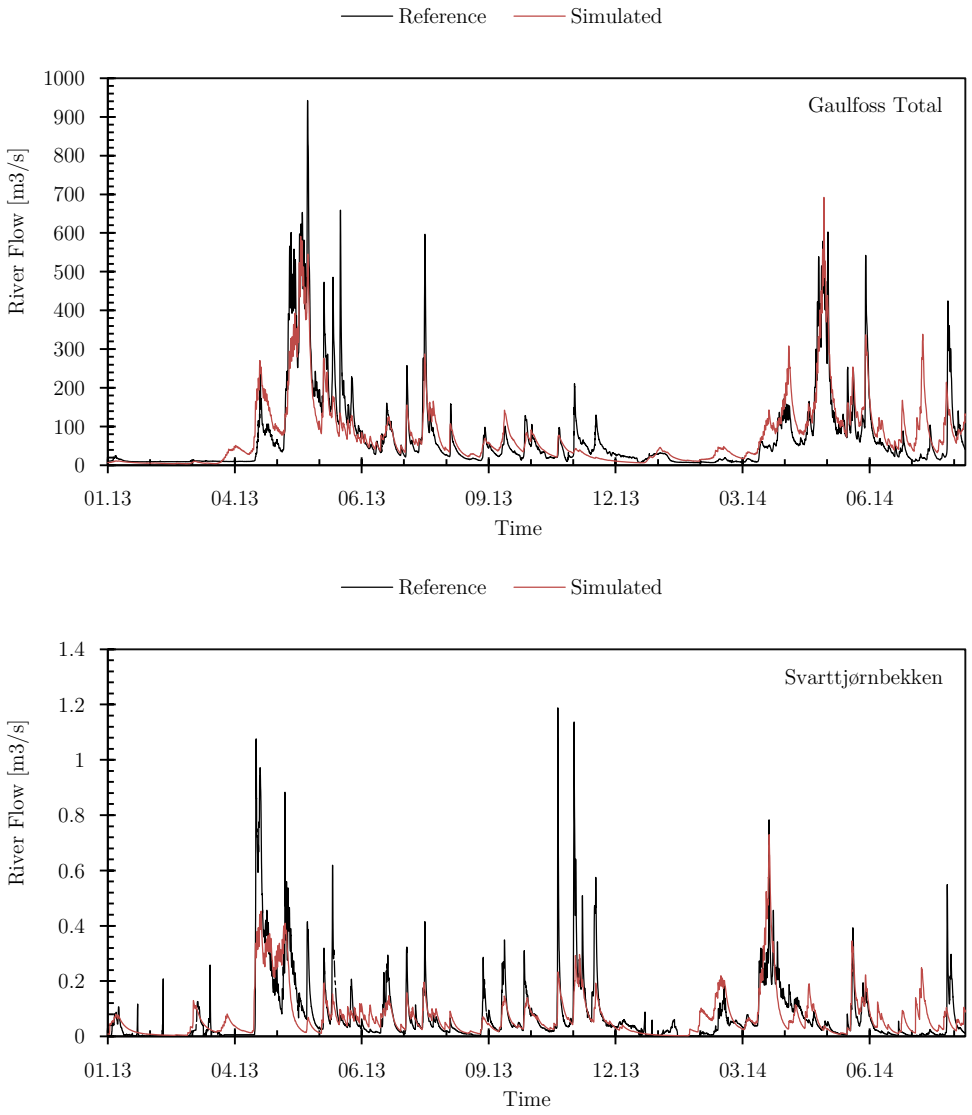

Figure 20. Flow simulation with distributed model including precipitation, temperature and wind measurements.

3.6.1 Parameters' Sensitivity

The results from a paremeter's sensitivity point of view are quite different to what was found for the PIHM model. One main difference involves the Windscale parameter, that probably thanks to the distributed windspeed input has now a more defined optimum.

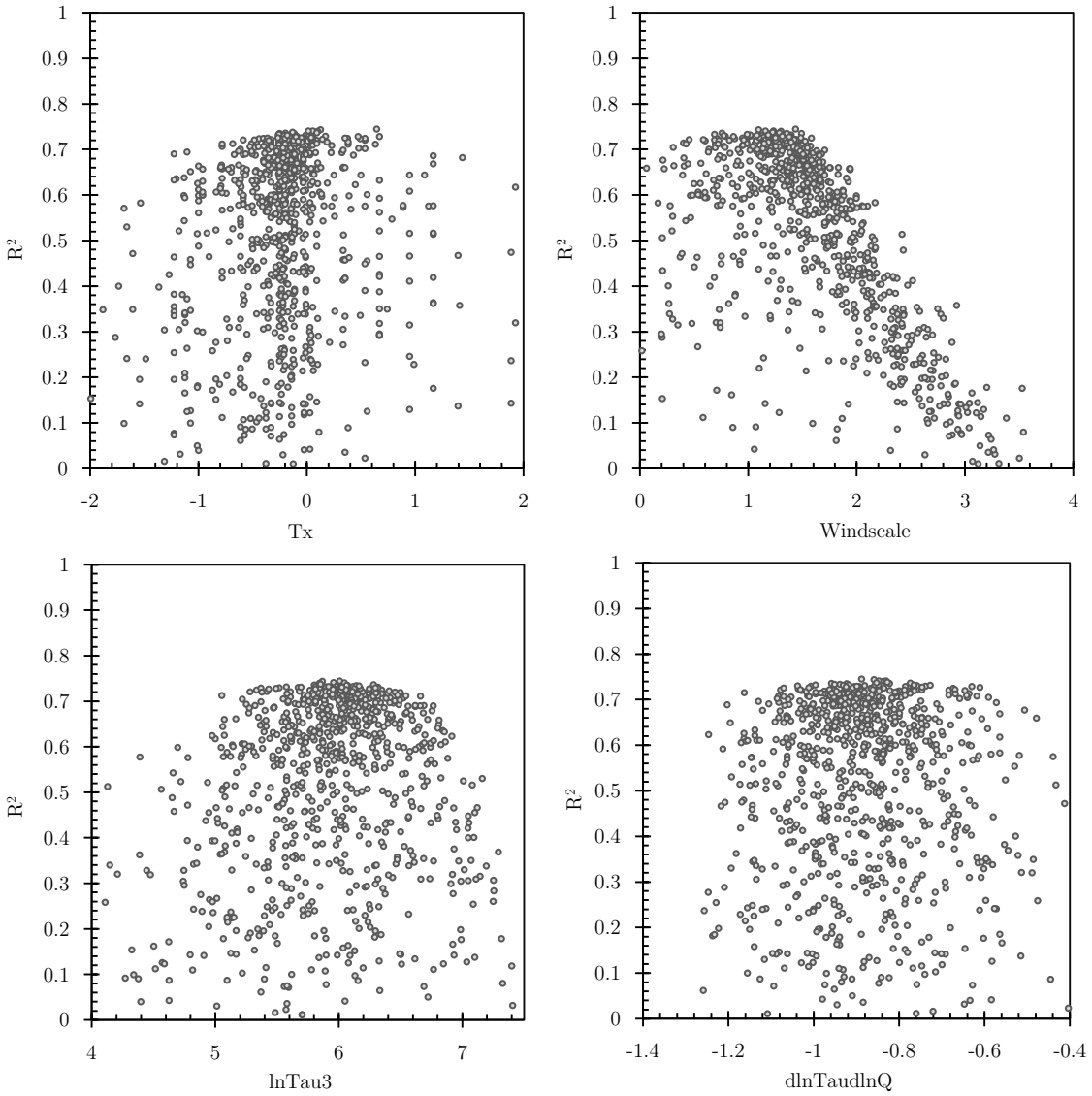

Figure 21. Parameter sensitivity for the Gaulfoss catchment in the setup including wind speeds.

Also the Tx parameter seems slightly more defined. Unfortunately though, the lnTau3 lost in this calibration run the clear optimum range that was found in the PIHM model. This results only show how much difficult it is to solve the problem of regionalization and how calibration and input dependent are these parameters.

3.7 Apriori Estimation of Parameters vs Calibration

The parameters for the Kirchner routine (lnTau3 and dlnTaudlnQ) are extracted from Figure 16 for the Gaulfoss catchment. Once these two are locked, only five parameters are left to be calibrated. The PIHM model with all the available stations has been used.
The results show comparable performances, with only minor losses.

	R2	lnR2
Gaulfoss Total	0.76	0.69

Table 5. Nash-Sutcliffe coefficients for the PIHM model with estimated Kirchner parameters.

It should be stressed though that, as discussed in Chapter 3.4.1, only those timesteps during nighttime hours with no precipitation are considered in analysis of the discharge data. Thus only 2 years of measurements were generally not enough for having a good fit in the linear regression; furthermore it has not been possible to properly bin the averages of the flow recession plot as described in Kirchner's paper (J.W.Kirchner, 2009) for this same reason. In general though, having the possibilities of estimating the response function's parameters a priori represents a huge advantage as described in Chapter 3.8.

3.8 Why a Minimalistic Approach

Calibrating the parameters of a hydrological model is an optimization problem that can, in certain cases, contain a high number of free variables (i.e. more than 10 or even 20). Such parameters are then evaluated comparing the simulated hydrograph with the observed river runoff; the information contained in the observed discharge, though, is not sufficient to estimate a single set of parameters than better describes a region. This translates in the equifinality problem, where many parameter sets achieve comparable levels of performance (Beven, 2005). Equifinality is generally caused by mutually compensating parameters (the increase in the value of a parameter can be compensated by modifying another one) or by parameters that are not very influencial and thus not easily definable. Furthermore, considered the high number of parameters to calibrate, the amount of possible combinations of values is tremendously big. To better express this concept it should be considered that, given a calibration problem with two parameters and a given objective function to optimize, if one had to discretize the parameter space into 100 parts it would end up with a total of 10000 combinations to try. Considering the currently popular HBV model, around 15-20 parameters are generally calibrated; this would imply an overwhelming 100^{15}-100^{20} possible combinations. Refer to Figure 22 for a visual representation of these concepts.

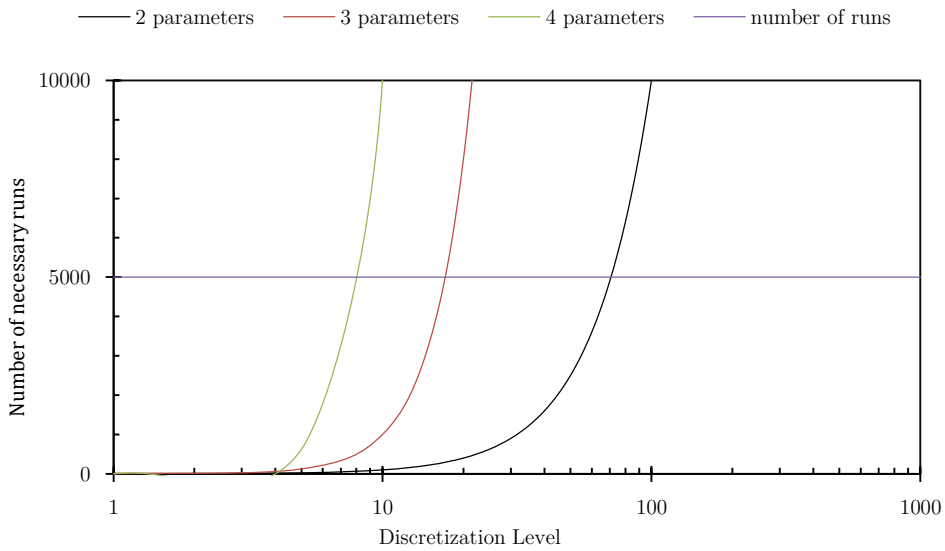

Figure 22. The figure visually shows how the number of runs necessary to cover every possible combination of the parameter space increases with the number of calibration variables and discretization level.

Thus, the calibration algorithms were developed to try to efficiently find the maximum of a given performance function without testing every possible combination. The lower the number of free parameters, to more likely the algorithm is to find the global (and not local) maximum of the objective function; furthermore such variables tend to become more independent reducing compensation problem. This allows to find parameter values that are a more "true" representation of the physical processes behind a catchment's response and, hopefully, that are more stable also in simulation runs outside the calibration timeframe (for example the validation period). Moving towards the direction of more minimalistic models will help in getting closer to a solution to the regionalisation problem, still widely open.

Chapter 4

Flood Forecasting System

4.1 Point flow forecasting

4.1.1 Background conditions

The reason why ENKI has been the perfect platform to perform the development and tests described by this thesis work is because, as previously mentioned, it not only allows distributed modelling, but also the freedom to create new routines that become part of the final model. During a simulation, the main result that is produced at the end of each time step is the GridRunoff raster, which represents the amount of runoff that is produced individually by each cell. The importance and limitations of this output are the two main concepts this chapter is based on; being able to calculate with such resolution the response of an area to meteorological inputs allows to transpose the scale of the analysis from a regional to a local point of view.

4.1.2 Purposes

Distributed models simulating grid runoffs allow to cover a lot of different tasks. An automated forecasting system could be developed in order to control and monitor sensible structures or areas such as bridges or mountain sides, allowing for evacuation plans or preventive measures to tackle flood scenarios. Simulations could be run on historical data to find out the return period of a certain event that occurred or the highest possible flow for dimensioning purposes. By applying regionalisation concepts and methodologies, it could also be possible to determine the effect of land use changes, which could help the planning stage of urban development. Also, by knowing the flow in every point of a river, it would be possible to check if environmental flows will be respected, given certain production plans and expected precipitation events. Lastly, for hydropower companies it could be a tool that allows to keep track of the expected inflow to a reservoir, the possibility of spills, the amount of water that can be transferred through waterways and so forth.

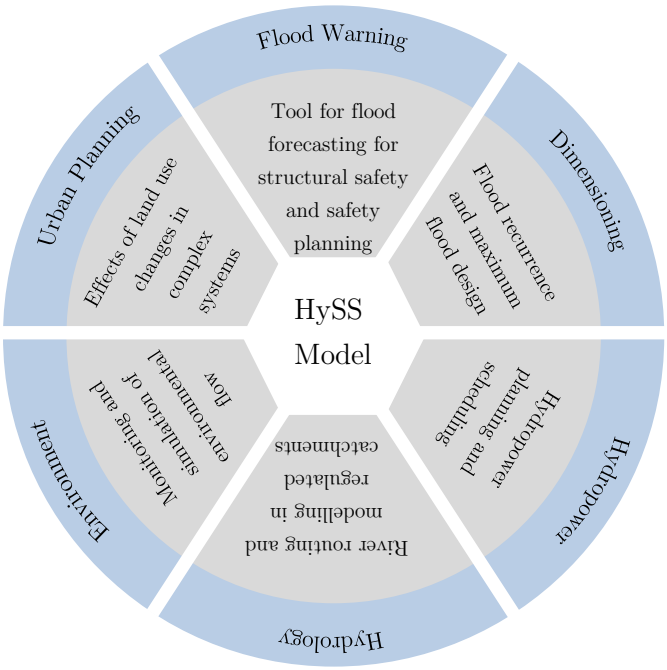

Figure 23. Visual representation of the possible applications of a comple point inflow model.

4.1.3 Needed development

Although a lot of potential resides in the information provided by the GridRunoff raster, improvements and additions need to be done in order to utilize it for Point Flow Forecasting. As the runoff is an aggregated response of a certain area it is needed to not only know the output from each cell, but also what happens upstream of them. In other words, it is important to define for every given point its contributing upstream catchment.

For this purpose one needs to know the flow patterns within the region. Most of the rivers of industrialized countries present some sort of regulation and completely natural areas are increasingly becoming more rare. As a result, in order to dynamically define the catchment area for each desired point, the model should contain a representation of the major components that influence water availability and distribution. In Norway in general and in the area studied, hydropower development represent the most important source for energy production. In the Nea-Nidelva catchment, north of Gaula, many major reservoir and power plants cover the area, and a number of water transferring system are altering the normal course that rivers would have in natural conditions. Furthermore, the presence of dams and reservoirs represent an obstacle for streams that must be taken into consideration.

A new routine HySS (see Chapter 4.2) has been coded in order to incorporate such components into the modelling system.

4.2 The hydropower system simulator (HySS)

HySS has been developed as a separate routine in ENKI using C++ programming. Its aim is to include into the modelling processes the main units of a hydropower system that

influence water distribution either by transferring or by storing it. This step is necessary to simulate inflow in specific points of a catchment that include these units.

4.2.1 Main components

HySS represents and describes the main mechanisms that are defining the flow of water. It is possible to make a distinction between two main groups:

- Independent mechanisms, including water flow through hillslopes and rivers following the highest gradient direction and water transferring systems.
- Dependent mechanisms, including flow bypass, flow release from a reservoir for energy production and the spill from spillways that naturally occurs when a reservoir level reaches a certain value.

The main difference between these two groups, is that the first group represents those mechanisms that are always present independently from the current time step or from any other external input. In theory water transferring systems should not be included in this category, since their operation depends on production plans, but for the purpose of this thesis, it has been assumed that all the water that flows into the intake of a waterway is transferred to its outlet, thus not accounting for minimum flow requirements or any external decision. On the other side, the second group represents those mechanisms that require additional information (bypass and production time series) or that are dependent on the specific time step (spill).

4.2.2 Theory of the HySS routine

The HySS routine works primarily by mapping the flow pattern within a region. In completely natural conditions, this would only be dominated by local topography, as water would tend to flow towards the point with the highest gradient. To represent this process, HySS uses the "Flow Direction" raster, which is obtained by using the relevant ArcGIS software's tool on a sinkless DEM with the same resolution as the region modelled in ENKI. The result is a raster that specifies cell by cell, with an integer ID value, what is the direction with the highest downfall gradient, as shown in Figure 24. Such numbers are specific of this processing tool in ArcGIS.

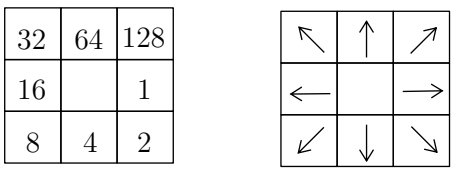

Figure 24. (left) Border cells contain the integer ID value that the center cell would be assigned with if water would flow towards their direction. (right) Conceptual representation of a cell of the "Flow Direction" raster.

As discussed in Chapter 4.1.3, the presence of artificial structures of a hydropower system modified the natural course of water; thus, representing flow patterns only with a "Flow Direction" raster would lead to erroneous results. Water transferring systems alter such pattern by moving water between two different cells that would not otherwise be connected. When water is transported from the intake of a waterway to its outlet, it continues its normal path following the gradient. When a dam is encountered, the water flow stops its course. From here on, two processes are described that enable water to flow past a dam: these are the spill that occurs when the water level of a reservoir reaches the spillway elevation and the production/bypass flows that are decided by the production plans of the energy companies. These are loaded in ENKI as input timeseries. All the cells that contribute to the flow to a reservoir are aggregated to form its inflow catchment. Similarly all the cells that contribute to the flow to the intake of a waterway form its watershed.

Downstream of a dam, the flow in each point is calculated as a sum between the local contributing area (excluding the upstream catchment of the dam) and the releases/spills from the reservoir.

The routine is thus able to calculate for each point in a river the actual flow, incorporating in the simulation the artificial components of a region. Furthermore, by knowing the contributing catchment to each reservoir, the routine is capable of calculating water mass balances in order to keep track of the stored volume of a reservoir and thus its height (if a volume-height curve is known). Knowing these informations is necessary since reservoirs and lake are of primary importance in a flood situation for their dampening effects.

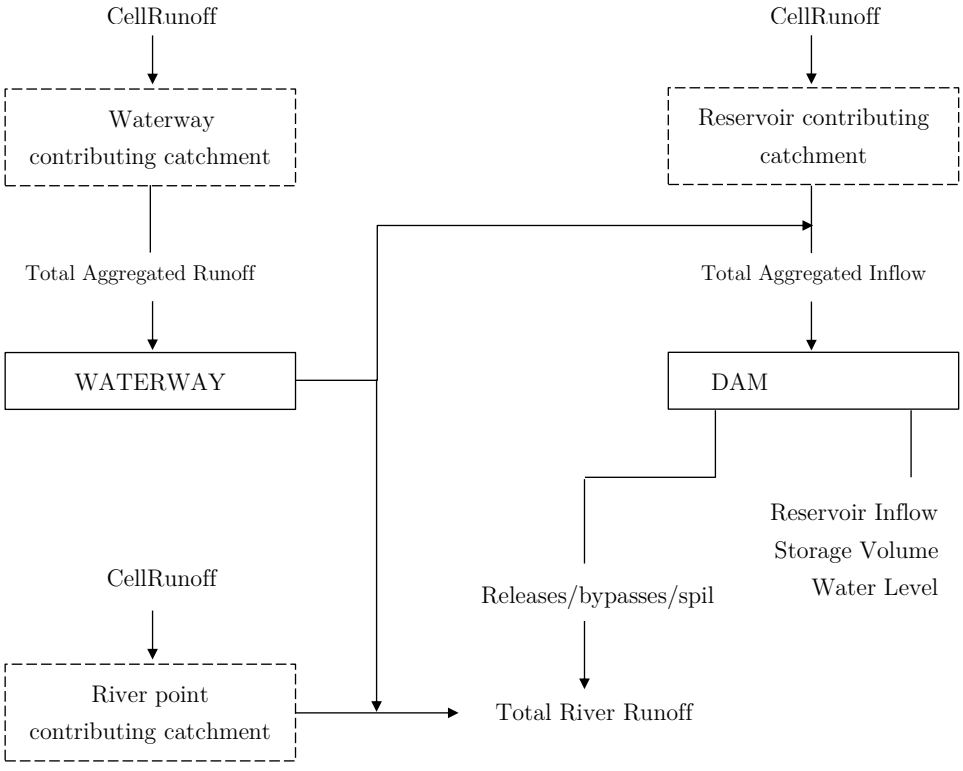

Figure 25. Conceptual representation of the HySS routine components

As made evident by Figure 25, the HySS routine can be used not only for flood forecasting in specific points of a region, but also as a tool for decision making within a hydropower operation context.

4.3 Future Developments

As HySS has been developed in this Thesis work in a simplified manner to provide a direct solution of the required tasks, it still needs further development in order to be complete and possibly used operationally. First of all there is a need to include all the components of a hydropower system. Waterways should be provided with a highest limit of capacity and/or timeseries indicating historical values of transferred water. Pumping options are not taken into consideration, and in some systems would make the current HySS insufficient to run a proper simulation. Another problem arises with the feature included in HySS that makes it able to automatically create catchment areas for each point one is interested in simulating. From tests conducted in the Nesjøen reservoir, the resolution of 1 squared kilometre is not enough to accurately map the flow direction. The ArcGis tool Flow Direction requires a sinkless DEM in order to run, the problem arises when createing a sinkless DEM, as the filling process conducted on such a coarse raster may end up with erroneous results. In this particular case, water was erroneously expected to flow out partly to the southern reaches of the reservoir and partly to the western parts, dividing the actual flow stored into the lake. A possible solution could be to implement a method that calculates the catchment boundaries on a higher resolution surface raster first and afterwards convert it into the required coarser resolution. Otherwise such task could be manually done by the user in the pre-processing phase.

Another important feature lacking in the present version of HySS is routing lake responses and river delays. This could be fundamental when analysing floods and their propagation through water bodies.

Chapter 5

Study Cases

5.1 Trondheim's Flood

5.1.1 Event Description

On the 12 August a high intensity precipitation event took place in an area between Tiller and Trondheim. Five measuring stations from the Norwegian Meteorological Institute were used to collect data regarding the event. The high density of observed data, considering the limited area, has allowed to get a clear idea on the development and characteristics of the event. Figure 26 shows an overview of the location of the observations. In particular, the Romulslia area has been recorded to have had flood problems in the sewage system because of the local intensity of rainfall; in the map, it is indicated with a square with a dotted perimeter.

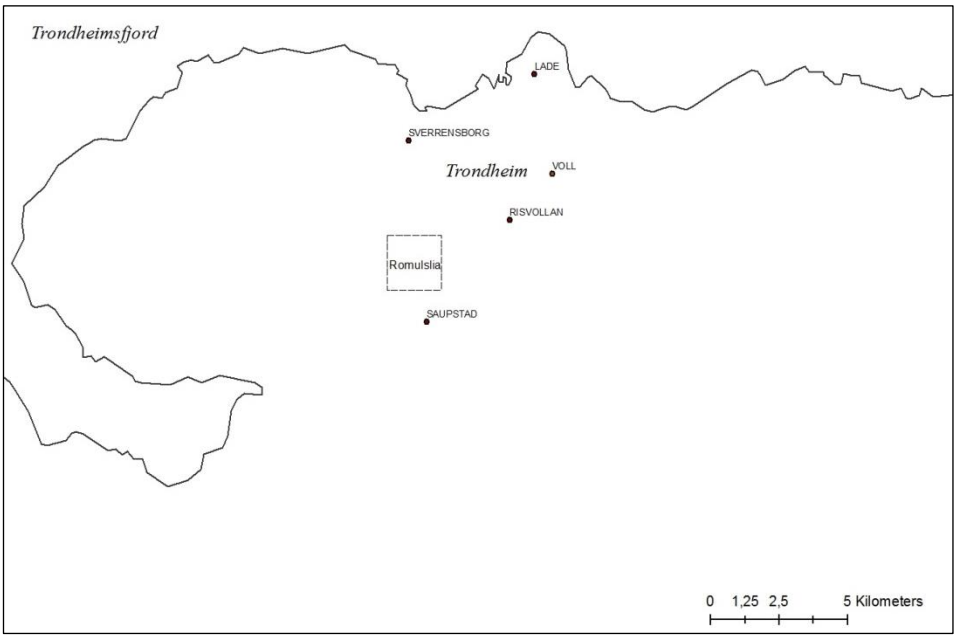

Figure 26. Overview of the study case area.

The precipitation took place in a moment when the antecedent moisture condition of the terrain was low due to the lack of rain during the days preceding the event. This slightly delayed the start of high runoff values.
It is important to notice that the hydrological model used does not include any representation of the different kind of artificial terrains that are present in an inhabited place; cement and asphalt, not being permeable, increase the amount of rainfall that directly converts into overland runoff. To try to simulate such behaviour, the two main parameters of the response function (lnTau3 and DlnTaudlnQ) were set to values that create a quicker response. Though it should be noted that the main purpose of this case study is not to evaluate the exact amount of runoff produced by an extreme event, since anyway there is no meter for comparison as no direct runoff measurements were taken during that day, but rather to give an assessment of the level of precision and reliability that can be locally obtained using forecasted inputs, especially precipitation. For simulation in larger catchments, knowing the exact location of a precipitation event could be of less relevance, since the final runoff is an aggregated measure of the behaviour of a larger extension of territory. Trying to simulate where in a city one can expect a flooding event, for example of the sewage system, due to locally high precipitation is another problem which is harder to tackle because of higher precision requirements.

Table 7 gives an overview of the development of the rainfall through the day. The much higher total values found in Saupstad and Sverrensborg are indicative of the fact that the precipitation was concentrated mainly on the Sout/Sout-West parts of Trondheim. The 54.6 mm measured in Saupstad in 24 hours represents a rainfall intensity with a return period of 20 years, based on data from the Trondheim municipality (Table 6**Error! Reference source not found.**), while the other events have a return period of less than two years, except from Sverrensborg with two to five years return period.

Returperioder(år); Nedbørsum(mm)
68862 TRONDHEIM - VOLL MOHOLT TYHOLT
Periode: 1967 - 2009
Antall sesonger: 39

År	1 min.	2 min.	3 min.	5 min.	10 min.	15 min.	20 min.	30 min.	45 min.	60 min.	90 min.	120 min.	180 min.	360 min.	720 min.	1440 min.
2	1,0	1,6	2,1	2,8	4,1	5,1	5,7	6,7	7,9	8,8	10,3	11,7	14,1	20,1	27,2	34,6
5	1,3	2,2	3,0	4,1	5,6	6,5	7,2	8,2	9,8	11,1	12,9	15,2	18,4	25,9	34,6	43,2
10	1,6	2,7	3,6	4,9	6,5	7,5	8,2	9,2	11,1	12,6	14,7	17,6	21,2	29,8	39,3	48,4
20	1,8	3,1	4,2	5,6	7,4	8,4	9,2	10,2	12,3	14,1	16,4	19,8	23,9	33,5	43,6	54,4
25	1,9	3,3	4,4	5,9	7,7	8,7	9,5	10,5	12,7	14,6	17,0	20,5	24,7	34,6	45,4	56,2
50	2,1	3,7	5,0	6,7	8,6	9,6	10,4	11,4	13,9	16,0	18,6	22,8	27,4	38,2	49,7	61,3
100	2,4	4,1	5,6	7,4	9,5	10,5	11,3	12,4	15,1	17,4	20,2	24,9	30,0	41,7	54,0	66,5
200	2,6	4,5	6,2	8,2	10,4	11,4	12,2	13,3	16,3	18,8	21,9	27,1	32,6	45,4	58,3	71,7

Table 6. Return periods for different rain intensity and time frames. Source: Trondheim Kommune.

Time	VOLL	LADE	RISVOLLAN	SV.BORG	SAUPSTAD
11.08.2013 23:00	0.78	0	0	0	0
12.08.2013 00:00	0.78	0	0	0	0
12.08.2013 01:00	0.78	0	0	0.4	0.1
12.08.2013 02:00	0.78	0	0	0.1	0.3
12.08.2013 03:00	0.78	0.1	0	0.4	1.1
12.08.2013 04:00	0.78	0.5	0.2	3.4	4.5
12.08.2013 05:00	0.78	1.5	2.1	3.3	2.4
12.08.2013 06:00	0.78	0.2	1.4	1.6	2.2
12.08.2013 07:00	0.78	0.2	1.2	0.7	1.1
12.08.2013 08:00	0.78	0	0.2	0.2	0.3
12.08.2013 09:00	0.78	0.2	0.1	1	2.5
12.08.2013 10:00	0.78	0.1	0.8	0.4	0.6
12.08.2013 11:00	0.78	0.1	0.1	0.1	0.4
12.08.2013 12:00	0.78	0	0	0	7.7
12.08.2013 13:00	0.78	0.3	0.4	0.4	4.8
12.08.2013 14:00	0.78	3.1	8.3	4.6	5.7
12.08.2013 15:00	0.78	1.8	6.9	2.3	2.5
12.08.2013 16:00	0.78	0.1	0.1	0.1	0.3
12.08.2013 17:00	0.78	10	3.8	10	10.3
12.08.2013 18:00	0.78	2.1	8.6	3.6	2.7
12.08.2013 19:00	0.78	1.2	0.2	2	1.5
12.08.2013 20:00	0.78	0.7	0	1	1
12.08.2013 21:00	0.78	0.3	0.8	0.5	0.7
12.08.2013 22:00	0.78	0.4	0.2	0.5	0.4
12.08.2013 23:00	0.78	0.9	0	2.4	1.5
SUM	19.5	23.8	35.4	39	54.6

Table 7. Observed precipitation by DNMI's stations in Trondheim. Voll shows daily record.

5.1.2 Simulating with AROME data

As stated in the previous Chapter, the main purpose of this case study is to answer to the following question: is the AROME data, especially the precipitation, reliable and precise enough to be used for flood forecasting purposes at a small (i.e. city) scale?

Two simulations were carried out, using both AROME and observations to try to compare the results of both the interpolated precipitations and the resulting runoff. As shown in Table 7, 2pm and 5pm were the hours with the most total precipitation.

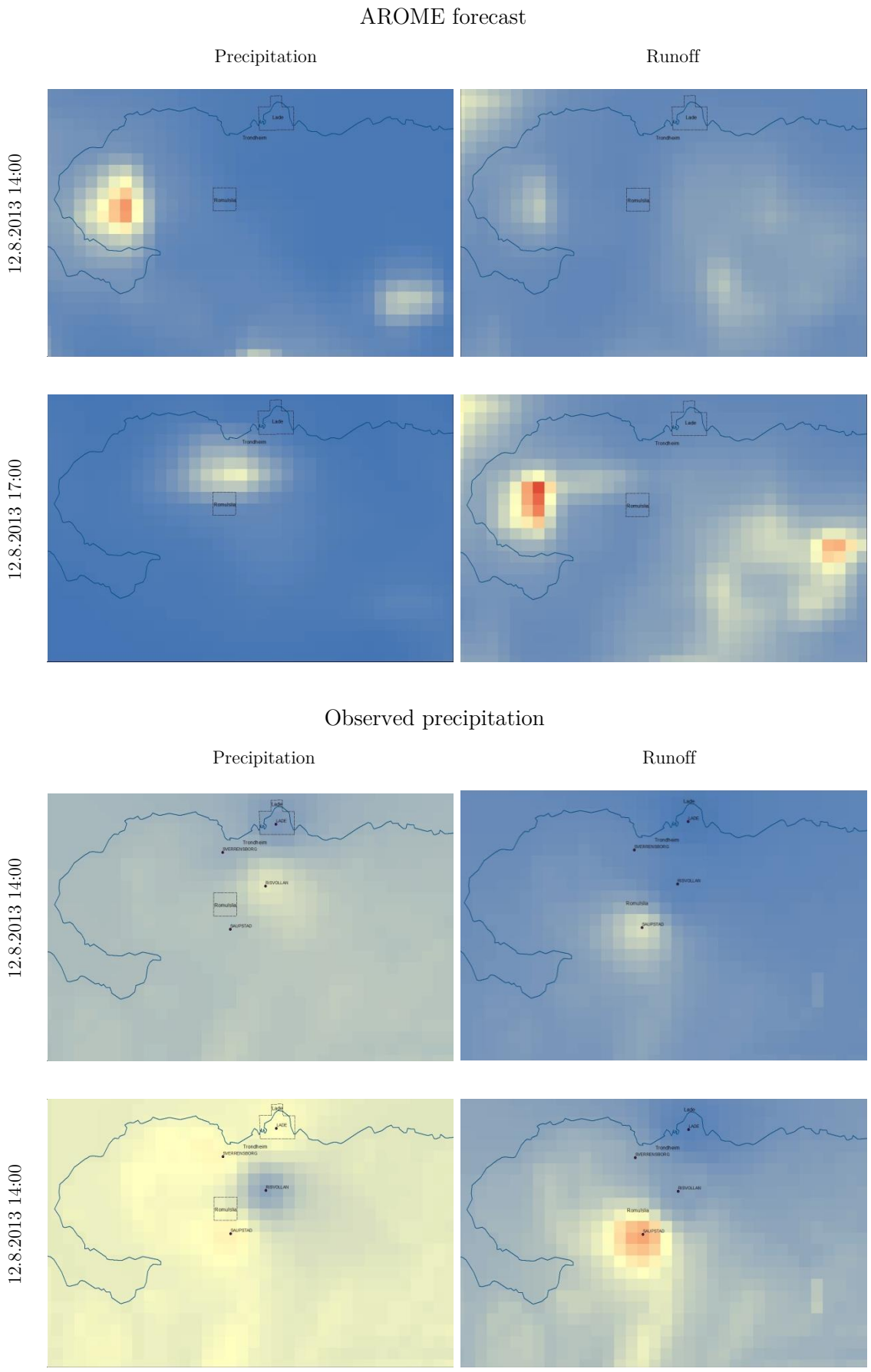

Figure 27. Precipitation and corresponding runoff responses for two timesteps, with and without distributed data.

From Figure 27 it is noticeable how the forecasted precipitation was expecting rainfall to happen circa 10km more towards the western sides of the city if compared to what observations show. During the day, then, the rain cloud moves towards the centre of Trondheim, but in the AROME data the precipitation is already weakened and its intensity much lower than the peak of the previous hours. On the other hand, in the observed data, rainfall covers a good deal of the municipality, leaving out its eastern side (Trondheim Voll's station). The resulting runoffs are quite different, with the area more hit by the event being shifted eastwards.

This test case proves that even though comparable calibration results are achievable using distributed data from six hours forecasts, the precipitation inputs can be considered somehow reliable if an idea of the amount of precipitation is needed, while poor results can be expected if such data has to be used for highly local events as in this case. This is still in line with the expectations had at the beginning of the thesis's work: it is still nowadays difficult to produce detailed forecasts, especially for precipitation, that can be used reliably for analysis with a resolution of few kilometres.

5.2 The upper Nea-Nidelva hydropower system

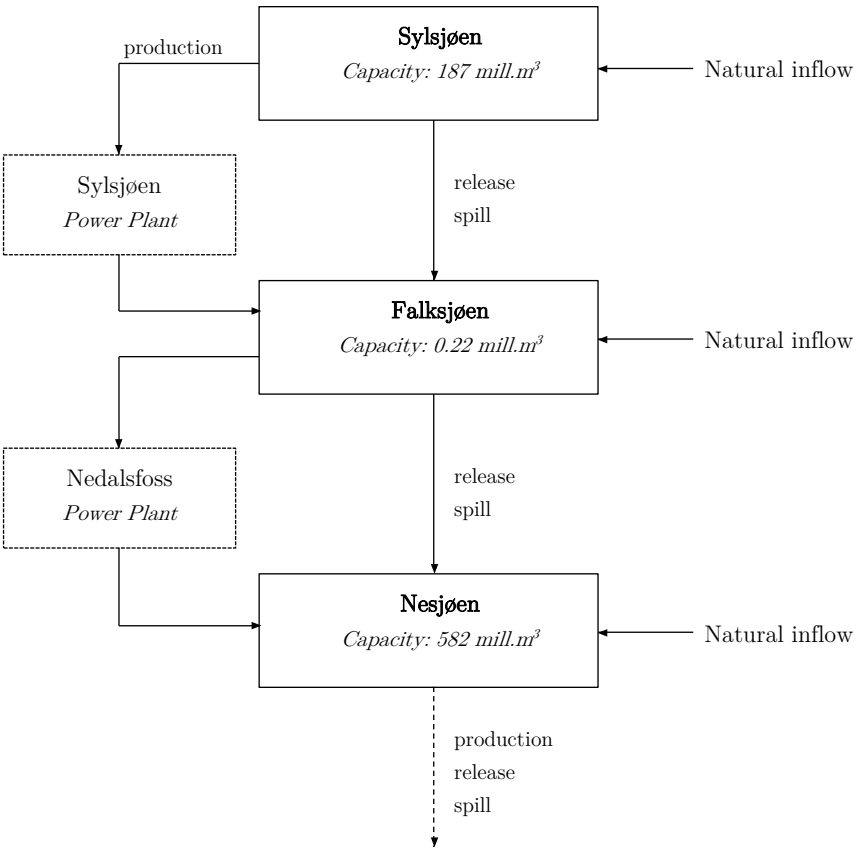

Figure 28. Schematical representation of the simulated hydropower system.

In a country with a heavy presence of hydropower developments like Norway, a flood forecasting system cannot be considered complete without integrating the main infrastructures of the power production; this is because the flow in most of the rivers is not completely natural, as it is a combination between the contribution from the local catchment, the releases from upstream reservoirs and eventually waterways that transfer in or out the water. As described in Chapter 4.2, an ENKI routine called HySS (HYdropower System Simulator) has been coded in order to fulfil this task.

The model has been then set up for the Nea region, at the border between Sweden and Mid-Norway. The system is composed of a series of three reservoir with three power stations. For each reservoir, HySS calculates the natural inflow coming from its local catchment and the corresponding variation in both the water storage and the water level. To do so, a simple water balance equation is considered:

$$V_t = V_{t-1} + I - E - P - B - S$$

$$S = f(H)\,, H = f(V)$$

V_{t-1} and V_t [Mill.m^3] represent the volume at the previous and current timestep. I and E [m^3/s], respectively the local inflow and the evaporation from the reservoir, are calculated by the Kirchner routine. In a reservoir, the evaporation is considered to be equal to its potential value since it comes from a body of water. No representation of surface ice and snow accumulated on top of it is included, therefore there might be an over estimation of the water availability during winter. P and B [m^3/s] represents the water that is released into the turbines for power production and the total bypasses; these are given inputs that have been taken from Statkraft's database. S is the spill in [m^3/s]. This could also be taken as input from a database, but since it is described by available simple equations, it has been implemented in order to be calculated automatically by the HySS routine. The spill is a function of the water level, which is calculated from the stored volume. The level-storage curves were also taken from Statkraft's database. As shown in Figure 29, level-spill curves were interpolated with a second order polynomial equation, while the more complex level-storage curve was interpolated with a third order polynomial equation, which gives good approximations at high capacities but a somehow poor representation at lower storage values.

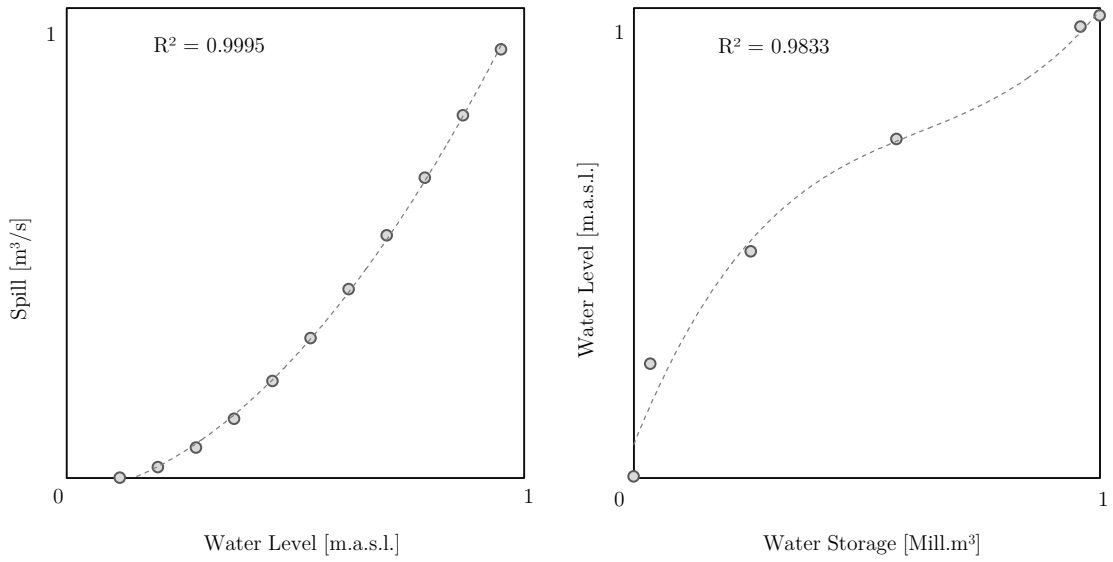

Figure 29. Normalized level-spill and level-storage curves.

The natural local inflow simulated has been compared with the data from Statkraft's database. It is here important to note that Statkraft's timeseries comes also from a water balance equation, the difference being that while HySS is calculating the storage from simulated inflows, Statkraft's series are calculating the storage through water level measurements. A problem arises at this step, for which one should pay attention when evaluating the results, and is that for reservoirs with a considerable surface, a small error in the readings (for example caused by winds that are increasing the water height on one side of the reservoir or simply by faulty instrumentation) can represent an erroneous water storage, since the volume error is the product between the height error and the surface.

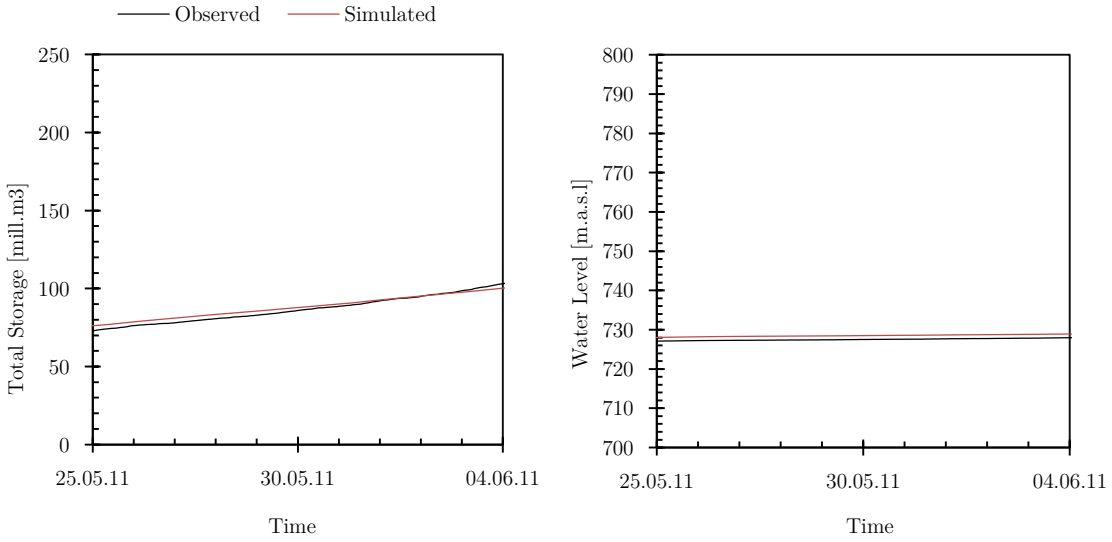

Figure 30. Storage (left, Sylsjøen) and water levels (right, Nesjøen) for a 10days snowmelt period.

As seen from Figure 30, there is a consistency between the observed water level or storage and the simulated ones, showing the effectiveness of the HySS routine. During the simulated period no spill has been registered both by HySS and by the observations at the dams.

The first simplified version of HySS has thus proved to be a reliable and useful tool to simulate the dynamics of a hydropower system. In a forecasting situation, for obvious reasons no observations of releases and production are available; what could be used in this case would of course be the production plans. In many countries in the world reservoirs not only fulfil the purpose of power production, but are also used for their flood dampening properties. Thus a tool that enables to calculate the resultant water flow at any point in a river downstream of a power system while at the same time keeping track of the variation of the water stored in a dam, is a useful tool to plan water management both for generic purposes but also for emergency situations were a limited release is needed not to overflow the downstream rivers while still avoiding to overtop a dam.

Chapter 6

Conclusion and Recommendations

6.1 Conclusion

This thesis work had the purpose of creating a hydrological forecasting model that could run using the highest resolution meteorological inputs available, DNMI'S AROME model, coupled with a routine in the ENKI hydrological framework that could simulate the main components of a hydropower system; this would enable to calculate the flow of a river, and thus floods, by taking into consideration also the production plans of these systems, which influence the natural flow.

Since no hourly observation database was available from the Norwegian Meteorological Institute, the first six hours of each updated forecast has been used: these distributed inputs to the hydrological models proved to be of satisfactory quality. In particular, temperature data proved to be extremely close to the interpolations made from observations. Including scaled wind data improved calibration performance and provides a good alternative in case measuring stations are not present. On the other hand precipitation data, the most important one, has shown to be overestimating actual rainfall trends if compared to meteorological stations in the area. Furthermore, as seen in the Trondheim's flood case study, the precision at which rain clouds are modelled is not yet sufficient to support a reliable use of this data for simulations during historical periods; though, for forecasting purposes, there are at the moment no better alternatives. Still, if compared to the model using observed data, using the distributed inputs from AROME with windspeed does not decreases the performance in terms of the Nash-Sutcliff coefficient. This leads to think that if the AROME model had included also Statkraft's and NVE's station, better results could be reached. Furthermore, calibrating with these kinds of data is recommended if the model has to be used for forecasting, since the parameters from the calibration of the model with observed data may be quite different. Thus all in all the performance achievable with AROME's data is more than satisfactory (especially in larger catchments where the exact location of a rainy event is less relevant) in a forecasting context, while still good for historical periods even though using observations increases the model's precision.

In order to use an hydrological model for forecasting floods in a river, the HySS (Hydropower System Simulator) has been coded to include in ENKI the main components of an hydropower system that influence the flow in a water body. The results show very good matches between simulated and observed water storage values in the reservoirs, as well as their local natural inflow.

6.2 Recommendations

The analysis done for both Svarttjørnbekken and Gaulfoss are influenced by the suspected quality of the data. Therefore studies on a larger pool of catchments are necessary to assess the quality and reliability of AROME's data and their usability in hydrological forecasting. Especially it is important to evaluate the precipitation input, which is by far the most important, and test methods for improving it.

REFERENCES

Bartholmes, J., & Todini, E. (2005). Coupling meteorological and hydrological models for flood forecasting. *Hydrology and Earth Systems Science*, 333-346.

Bergstrøm, S., & Forsman, A. (1973). Development of a conceptual deterministic rainfall-runoff model. *Nordic Hydrology*.

Beven, K. (2005). A manifesto for the equifinality thesis. *Journal of Hydrology 1-19*.

Bruland, O., Lena S., T., Engeland, K., & Kolberg, S. (2009). ENKI – Operational hydrological forecasting system. *17th International Northern Research Basins Symposium and Workshop.* Iqaluit-Pangnirtung-Kuujjuaq, Canada.

Duan, Q., Sorooshian, S., & Gupta, V. (1992). Effective and efficient global optimization for conceptual rainfall-runoff models. *Water Resources Research, vol. 28-04*, 1015-1031.

Friedl, M., & al., e. (2002). Global land cover mapping from MODIS: algorithms and early results. *Elsevier, Volume 83, Issues 1–2*, 287–302.

J.W.Kirchner. (2009). Catchments as simple dynamical systems: Catchment characterization, rainfall-runoff modeling, and doing hydrology backward. *Water Resour: Res., 45*.

Kolberg, S. (2006). Updating of snow depletion curve with remote sensing data. *Hydrologial Processes*.

Källén, E. (1996). HIRLAM documentation manual. *SMHI, Norrkoepping, Sweden*.

M.A Friedl et al. (2002). Global land cover mapping from MODIS: algorithms and early results. *Elsevier, Volume 83, Issues 1–2*, 287–302.

Nash, J., & Sutcliffe, J. (1970). River flow forecasting through conceptual models part I — A discussion of principles. *Journal of Hydrology, Volume 10, Issue 3*.

Pristley, C., & Taylor, R. (1972). On the assessment of surfaceheat flux and evaporation using large scale parameters. *Monthly Weather Review,100,*, 81-92.

Seity, Y., Brousseau, P., Malardel, S., Hello, G., Bénard, P., Bouttier, F., . . . Masson, V. (2011). The AROME-France Convective-Scale Operational Model. *American Meteorological Society, Volume 139, Issue 3*.

Shuttelworth, W., & Calder, I. (1979). Has the Priestley-Taylor equation any relevance to forest evaporation? *Journal of Applied Meteorology 18*, 639-646.

Stagnitti, F., Parlange, J., & Rose, C. (1989). Hydrology of a Small Wet Catchment. *Journal of Hydrological Processes,3*, 137-150.

Weiss, M., & Menzel, L. (2008). A global comparison of four potential evapotranspiration equations and their relevance to stream flow modelling in sem-arid environments. *Advances in Geosciences*.